Learning improves decoding of odor identity with phase-referenced oscillations in the olfactory bulb

Justin Losacco[1,2,*], Daniel Ramirez-Gordillo[2,*], Jesse Gilmer[1,3] and Diego Restrepo[1,2,#]

[1] Neuroscience Graduate Program

[2] Department of Cell and Developmental Biology

[3] Department of Physiology and Biophysics

University of Colorado Anschutz Medical Campus, Aurora, CO 80045, USA

[*] J.L and D.R.G. contributed equally to this work

[#] Corresponding author: Diego Restrepo, diego.restrepo@cuanschutz.edu

Abstract

Local field potential oscillations reflect temporally coordinated neuronal ensembles—coupling distant brain regions, gating processing windows, and providing a reference for spike timing-based codes. In phase amplitude coupling (PAC), the amplitude of the envelope of a faster oscillation is larger within a phase window of a slower carrier wave. Here, we characterized PAC, and the related theta phase-referenced high gamma and beta power (PRP), in the olfactory bulb of mice learning to discriminate odorants. PAC changes throughout learning, and odorant-elicited changes in PRP increase for rewarded and decrease for unrewarded odorants. Contextual odorant identity (is the odorant rewarded?) can be decoded from peak PRP in animals proficient in odorant discrimination, but not in naïve mice. As the animal learns to discriminate the odorants the dimensionality of PRP decreases. Therefore, modulation of phase-referenced chunking of information in the course of learning plays a role in early sensory processing in olfaction.

Significance

Early processing of olfactory information takes place in circuits undergoing slow frequency theta oscillations generated by the interplay of olfactory input modulated by sniffing and centrifugal feedback from downstream brain areas. Studies in the hippocampus and cortex suggest that different information “chunks” are conveyed at different phases of the theta oscillation. Here we show that in the olfactory bulb, the first processing station in the olfactory system, the amplitude of high frequency gamma oscillations encodes for information on whether an odorant is rewarded when it is observed at the peak phase of the theta oscillation. Furthermore, encoding of information by the theta phase-referenced gamma oscillations becomes more accurate as the animal learns to differentiate two odorants.

Introduction

Animals must modulate early sensory processing to optimize navigation of their environment (Gire et al., 2013a; Pakan et al., 2018). This experience-dependent shaping involves an interplay between sensory input, behavioral state, arousal and motor activity. Neuronal activity, temporally organized by local field potential (LFP) oscillations, carries distinct information at different phases of each cycle (Jensen, 2001; Kepecs et al., 2006; Lisman and Jensen, 2013). For example, in the hippocampus different phases of the theta LFP (2-12 Hz) preferentially encode present and future spatial locations, illustrating temporal “chunking” of information (Amemiya and Redish, 2018; Siegle and Wilson, 2014). Place cell preferred fields are encoded temporally through phase precession in relation to hippocampal theta oscillations (Buzsaki and Draguhn, 2004; Lisman, 2005; O'Keefe and Recce, 1993; Skaggs et al., 1996). Additionally, LFP oscillations in different frequency bandwidths can be related through cross frequency coupling (CFC), which can further enhance information carrying capacity (Canolty and Knight, 2010; Engel et al., 1999; Florin and Baillet, 2015; Fries, 2005).

One example of CFC is PAC, wherein the amplitude of a faster oscillation (e.g. gamma, 35-95 Hz) is related to the phase of a slower oscillation (e.g. theta, 2-12 Hz) (Chrobak and Buzsaki, 1998; Soltesz et al., 1993). PAC occurs during task engagement in rodent hippocampus (Bragin et al., 1995; Lisman and Idiart, 1995; Soltesz et al., 1993), rodent orbitofrontal cortex (van Wingerden et al., 2014), macaque auditory cortex (Marton et al., 2019), human hippocampus (Lega et al., 2016) and human visual cortex

(Daume et al., 2017; Seymour et al., 2017). Interestingly, Van Wingerden et al. (van Wingerden et al., 2014) described how theta-gamma PAC strengthens in rat orbitofrontal cortex with learning for trials in which the correct decision was made in the olfactory go no-go task.

The study of PAC in the earliest sensory processing brain areas is virtually non-existent. The olfactory bulb (OB) is an ideal location to study whether PAC is relevant to sensory processing; its intrinsic oscillatory activity is linked to odorant signal processing (Doucette et al., 2011; Gschwend et al., 2012; Li et al., 2015; Smear et al., 2011). The rhythmic activation of olfactory sensory neurons (OSNs) through breathing generates a theta-frequency (2-12 Hz) respiratory-related LFP in the target region of the OSNs, the OB, that is coherent with oscillations in downstream processing areas such as piriform cortex (PC) and hippocampus (Gourevitch et al., 2010; Heck et al., 2019; Nguyen Chi et al., 2016; Tort et al., 2018). Interestingly, PAC is present in human PC, and the respiratory phase for presentation of stimuli modulates the ability to retrieve episodic memory (Zelano et al., 2016). Downstream neural networks receiving olfactory information from the OB could be tuned to respond to sensory input at certain phases of this theta LFP (Buzsaki, 2010; Jensen, 2001) and could send back modulatory signals during other phases (Kay, 2015; Kepecs et al., 2006).

Decades of work have characterized LFP activity in the OB in various states of wakefulness (Adrian, 1950; Chery et al., 2014; Li et al., 2012) and olfactory task engagement (Gourevitch et al., 2010; Martin and Ravel, 2014). Surprisingly, this LFP

signal changes in response to prior experience (Courtiol and Wilson, 2017; Gire et al., 2013b). Work in the go no-go operant conditioning task where the animal learns to respond to the reinforced odorant for a water reward has revealed broadband LFP power changes for the rewarded versus the unrewarded odorant with discrimination learning (Beshel et al., 2007; Martin et al., 2004; Ramirez-Gordillo et al., 2018; Stopfer and Laurent, 1999). Additionally, changes in the balance of sensory and corticofugal inputs to OB interneurons can alter timing of beta and gamma oscillatory states, suggesting that information transfer from the OB is influenced by top-down signaling (David et al., 2015). Also, these investigators posited that slower theta oscillations gate temporal windows for sensory and centrifugal inputs to ascend and descend, respectively, suggesting an important role for PAC in gating information transfer. Since PAC exists in the OB in anesthetized (Buonviso et al., 2003) and awake, idle rats (Rojas-Libano et al., 2014), we wondered whether PAC changes with learning, reflecting unsupervised Bayesian learning or supervised learning through top-down modulation sensory information (Hiratani and Latham, 2019), and whether encoding this information by the power of high frequency oscillations differs as a function of the phase of the theta LFP.

Here, thirsty mice implanted with tetrodes in the OB learned to associate an odorant with water reward in the go no-go task, discriminating between two monomolecular odorants (e.g. between isoamyl acetate vs acetophenone, IAAP) or between a monomolecular odorant and an odorant mixture (between ethyl acetate and a mixture of ethyl acetate and propyl acetate, EAPA). LFP was analyzed over task

127 learning for changes in PAC and for the ability of theta phase-referenced high frequency
128 oscillatory power—termed phase referenced power (PRP) hereafter—to encode for the
129 perceived contextual identity of the odorant.
130
131 We demonstrate that the strength of PAC, quantified as the modulation index
132 (Tort et al., 2010), changes for the rewarded odorant (S+) as the animals learn.
133 Interestingly, the variance of the angle of theta with the strongest gamma oscillation
134 (peak angle) increases for the unrewarded odorant (S-) over the course of learning.
135 These changes in PAC raised the question whether a downstream observer focused on
136 high frequency oscillations at different theta phases would find a difference in stimulus
137 prediction with learning. We found that the ability to decode stimulus identity by PRP
138 improves with task proficiency and the dimensionality, a measure of separable
139 representation within signals, decreased as the animal learned to differentiate the
140 odorants, suggesting that a stable and unambiguous representation of odor identity
141 arises in PRP after learning.
142
143

Results

The experiments were designed to study encoding of odorant identity by cross-frequency coupling. We report data obtained in two different sets of experiments that we name Exp1 and Exp2. As shown in Table S1 the two experiments differed in electrode locations, mouse genotype, device implantation (tetrode vs. optetrode), and odorant pairs used (see also Methods). Mice learned to discriminate between rewarded (S+) and unrewarded odorants (S-) presented in pseudorandomized order in the go no-go olfactory task (Figure 1A-C). The dataset is comprised of 119 recording sessions in 30 mice. The odorant pairs tested were different volatile compounds (or mixtures) whose nomenclature addresses the odorant names and the experimental set (e.g. IAAPexp1, see Table S1 for the nomenclature). Table S2 enumerates the total number of sessions per odorant pair, mouse, and experiment.

In the go-no go task mice start the trial spontaneously by poking their nose into the odor spout and licking on the lick port. The odorant is delivered at a random time 1-1.5 sec after nose poke (the time course for odorant concentration is shown in Figure 1-figure supplement 1). The mice must decide to either lick a waterspout at least once during each 0.5-second bin in the 2-second response area (green blocks in Figure 1B) to obtain a water reward for the rewarded odorant or refrain from licking for the unrewarded odorant (Figure 1C). We did not punish for licking for the unrewarded odorant, and mice refrain because of the effort it takes to lick. Behavioral performance was termed naïve or proficient when their performance estimated in a 20-trial window

166 was ≤ 65% for naïve and ≥ 80% for proficient. After three 20-trial blocks of proficient
167 performance, the session was ended; valence was reversed the next day (not shown) or
168 another odorant was tested. We recorded the LFP using four tetrodes (16 electrodes)
169 implanted in the OB and we analyzed the data to determine whether information carried
170 by cross-frequency coupling can encode for the contextual identity of the odorant for
171 naïve or proficient mice. Importantly, reversal experiments from previous studies where
172 we switched the rewarded and unrewarded odorants have shown that the power of the
173 LFP in the OB and mitral/tufted cell spiking encodes for the *contextual* identity of the
174 odorant (is the odorant rewarded?)(Doucette et al., 2011; Doucette and Restrepo, 2008;
175 Li et al., 2015; Ramirez-Gordillo et al., 2018). Therefore, when we refer to identity in this
176 publication we do not mean the chemical identity of the odorant, we mean whether the
177 odorant is rewarded or unrewarded. Finally, to evaluate the statistical significance of
178 differences in oscillatory parameters estimated in this study the estimates were either
179 averaged in the time period of odorant application (0.5 to 2.5 sec after diverting the
180 odorant to the odor delivery spout) or the statistical significance was evaluated for the
181 entire time course with time points every 0.1 sec using a generalized linear model
182 (GLM, see Methods). Furthermore, we complement testing of statistical significance
183 using p values with estimation of bootstrapped confidence intervals (Halsey et al.,
184 2015).

185

186 **Phase amplitude coupling analysis of the LFP recorded in the go no-go**
187 **behavioral task**

188 In order to understand whether odorant identity is encoded by by cross-frequency
189 coupling in the OB we characterized PAC, which is a cross-frequency coupling
190 mechanism where high frequency oscillation bursts take place at specific phases of low
191 frequency theta oscillations (Tort et al., 2010). PAC has been reported in the OB
192 (Buonviso et al., 2003; Rojas-Libano et al., 2014), but has not been thoroughly
193 characterized. Figures 1D-E show our approach to quantify the strength of PAC using
194 the modulation index, a measure of how localized high frequency firing is within the
195 phase of theta oscillations. Figures 1Di and ii show an example of the extracellular LFP
196 sampled at 20 kHz and filtered between 1-750 Hz. The raw signal (Figure 1Di) was
197 filtered with a 20th order Butterworth filter into different LFP frequency bands (Figures
198 1Dii, iii and v) (theta, 6-14 Hz, adapted from (Nguyen Chi et al., 2016); beta, 15-30 Hz;
199 or high gamma, 65-95 Hz). Figures 1Diii and 1Dv show that the filtered theta and high
200 gamma LFP appear to change amplitude in a coordinated manner. We used PAC
201 analysis (Tort et al., 2010) to evaluate the degree of coupling of the amplitude of the
202 envelope of the beta or high gamma LFP on the phase of the theta LFP. Figure 1Div
203 shows the theta phase and the red line in Figure 1Dv shows the envelope for the
204 amplitude of the high gamma LFP, both calculated with the Hilbert transform as detailed
205 in Tort et al. (Tort et al., 2010). Figure 1E shows the phase amplitude plot of the
206 normalized distribution of high gamma amplitudes in different theta phase bins. For this
207 example there are two maxima, and the vertical red line corresponds to the phase of
208 theta at which the gamma amplitude is highest (at ~95 degrees); this is called the “peak
209 phase”. Similarly, the phase with the smallest normalized amplitude is called the “trough
210 phase” (vertical blue line at ~5 degrees). The strength of PAC was estimated as the

211 modulation index (MI), a measure computed as the Kullback–Leibler (KL) distance to
212 the uniform phase distribution normalized to range from 0 (uniform distribution) to 1
213 (sharp gamma bursts at a specific theta phase) (Tort et al., 2010). The MI for the
214 distribution in Figure 1E is 0.018. Figure 1-figure supplement 2 shows the LFP power
215 spectrogram for simulated data with low gamma oscillations that are either uniformly
216 distributed in the theta phase (MI=0.0004, Figure 1-figure supplement 2A) or with
217 gamma bursts at 180 degrees of the theta oscillation (MI=0.01, Figure 1-figure
218 supplement 2B). Recordings in hippocampus and cortex yield MI values in the range of
219 0.005-0.03.

220

221 **Peak angle variance for theta/high gamma phase amplitude coupling increases**
222 **for S- when the animals learn to differentiate odorants in the go-no go task**

223 We proceeded to ask whether the strength of PAC, quantified by MI, and the
224 peak angle change as the animal learns to differentiate odorants in the go-no go task.
225 Figure 2A-F illustrates theta/high gamma PAC for all S+ and S- odorant trials in one
226 session for a mouse proficient in differentiating the odorants. The phase amplitude plots
227 for all the trials are shown in pseudocolor in Figure 2A, behavioral performance is
228 shown in Figure 2B, and the corresponding normalized phase amplitude plots are
229 shown in Figure 2C, while the mean average theta LFP is shown for one cycle in Figure
230 2D. There is clear (biphasic) theta phase coupling for high gamma amplitude with
231 maxima at ~120° and 270° for S+ (Figure 2Ai and red line in 2C). This strong PAC is
232 reflected by an MI with a mean of 0.02 with small trial to trial variance (Figure 2E, red
233 circles), and small variation in peak phase (Figure 2F, red polar histogram). In contrast,

234 PAC displays variable strength and phase for S- in this session (Figure 2Aii, blue line in
235 2E and blue polar histogram in 2F). For S- the average MI is smaller and displays large
236 variance ranging from 0 to 0.06 (mean MI 0.014, Figure 2E, blue circles). The peak
237 angle for S+ takes place slightly above 90 degrees and varies significantly for S- (Figure
238 2F). The MI and peak angle variance differ significantly between S+ and S- (MI:
239 ranksum p value < 0.001, peak angle variance: ranksum p value < 0.05, n = 50 S- trials,
240 49 S+ trials).
241
242 Browsing through PAC data for different sessions, plotted as in the example
243 shown in Figures 2A-F, raised the question whether PAC changes over the course of
244 learning in the go-no go olfactory discrimination task—as reported by mean MI and
245 peak angle variance. We noticed that in sessions where the mouse learned to
246 differentiate the odorants the phase of the peak angle became highly variable when the
247 animal became proficient. An example is shown in Figure 2-figure supplement 1 where
248 a mouse started the session performing close to 50% correct, and became proficient
249 during the last portion of the session. The phase of the peak angle is highly variable for
250 the last 20 S- trials. We proceeded to estimate mean MI and peak angle variance for all
251 mice. The mean MI and peak angle variance was estimated as the mean in all trials
252 within either the naïve or proficient periods for S+ and S-, calculated between 0 and 2.5
253 sec after odorant application. Figure 2G illustrates cumulative histograms for the mean
254 MI (i,iii) and peak angle variance (ii,iv) for theta/beta (i,ii) and theta/high gamma PAC
255 (iii,iv) for the APEBexp1 odorant for S+ and S- odorants for trial ranges when the mice
256 were naïve or proficient. The cumulative histograms for mean MI measured per

electrode (Figure 2Gi,iii) show small yet statistically significant changes in PAC strength for both the theta/beta and theta/high gamma as the animal learns to discriminate between odorants (GLM analysis, indicates that the differences in mean MI in terms of proficiency and the event type are significant $p<0.001$, 896 degrees of freedom, d.f., for theta/beta and theta/high gamma, 16 electrodes per mouse, 14 mice). In addition, the circles in Figure 2Gi,iii show the per mouse mean MI. A GLM analysis did not yield significant changes for the per mouse average MI as a function of either event type or proficiency for theta/beta PAC ($p > 0.05$, 52 d.f., 14 mice). Per mouse average MI was significant for both event type and proficiency for theta/high gamma PAC ($p < 0.05$, 52 d.f., 14 mice). Finally, for the APEBexp1 odorant pair we found a substantial decrease in peak angle variance for S+ and an increase in peak angle variance for S- for both the theta/beta and theta/high gamma PAC (Figure 2Gii,iv, GLM analysis for changes in peak angle variance for both proficiency and event type yield $p < 0.001$, 892 d.f. for both theta/beta and theta/high gamma, 16 electrodes per mouse, 14 mice). The changes were also statistically significant when a GLM was computed for the average peak angle variance per mouse (circles in Figures 2Gii,iv, GLM p value < 0.01 for theta/beta and $p < 0.001$ for theta/high gamma for both event type and proficiency with 52 d.f.,14 mice).

Similar differences between S+ and S- and changes when the animal became proficient were found for peak angle variance for the other odorant pairs (Supplemental Information and Figure 2-figure supplement 2). Furthermore, we evaluated the changes in PAC strength quantified as MI and peak angle variance by analyzing per-experiment mean values (averaged over odorant pairs, Figure 2H). GLM yielded significant p values

280 for peak angle variance for theta/high gamma PAC for S+ vs. S- (< 0.01, 16 d.f.) and for
281 the interaction between S+ vs. S- and proficiency ($p<0.05$, 16 d.f.) (Figure 2Hiv). For a
282 downstream observer focused on the LFP power at the peak of PAC for the rewarded
283 odorant these changes in peak angle variance may reflect a mechanism by which the
284 unrewarded stimulus is devalued while the rewarded odorant is valued. To our
285 knowledge, this is the first demonstration of dynamic cross frequency interactions
286 changing with learning for early processing in sensory systems.
287
288 **Peak phase referenced power increases for S+ and decreases for S- over learning**
289 The existence and evolution of PAC over learning alone does not demonstrate its
290 potential utility to the animal in its decision-making process. In order to assess whether
291 high frequency LFP power at the peak of theta oscillations changes as the animal learns
292 we performed wavelet analysis to extract the power of high gamma (and beta) LFP
293 referenced to specific PAC phases of theta—peak and trough (as defined in Figure 1E).
294 We term this analysis phase-referenced (high-frequency) power, or PRP. PRP analysis
295 allows answering the question whether the power of burst high frequency LFP
296 evaluated at a specific phase for PAC changes as the animal learns to differentiate the
297 odorants in the go-no go task.
298
299 In Figures 3A-C, we show how this PRP analysis was performed. Figure 3A
300 shows Morlet wavelet LFP power analysis (Chery et al., 2014; David et al., 2015) for a
301 single S+ trial characterized by strong, persistent theta power during and after odor
302 delivery (related to respiration and olfactory investigation) accompanied by higher

303 frequency power bursts whose periodicity reflects PAC. Figure 3B shows the theta (6-14
304 Hz)-filtered waveform (Figure 3Bi) and the Hilbert-extracted phase (Figure 3Bii, (Tort et
305 al., 2010)) co-registered to the one-second epoch extracted from the wavelet LFP
306 power plot shown in Figure 3Aii. We proceeded to extract the value of the power (in
307 decibels) referenced to the peak or the trough of PAC measured in S+ trials (peak and
308 trough are defined in Figure 1E). The red line in Figure 3Ci shows a clear odor-induced
309 increase in the peak-referenced wavelet power for high gamma/theta PAC in this single
310 trial example (Figure 3Ci, red line). In contrast, there was little change in power
311 referenced to the trough of PAC (Figure 3Ci, blue line). Figure 3Cii shows the time
312 course for the average peak (red) and trough (blue) PRP calculated for all trials in this
313 go-no go session for a mouse that was performing proficiently in differentiation of the
314 two odorants.
315
316 In order to assess whether PRP changes with learning we performed this
317 analysis for all sessions for naïve and proficient periods. Figure 3D shows cumulative
318 histograms for the peak and trough PRP for all mice for the odor period for all go-no go
319 sessions with the IAAPexp2 odorant pair for theta/high gamma PAC. Over the course of
320 learning, peak-related high gamma power increases for S+ and decreases for S- (Figure
321 3D top). In contrast, the changes elicited by learning in trough PRP are smaller (Figure
322 3D bottom). The differences were statistically significant between peak and trough, S+
323 and S- and naïve and proficient (GLM p values < 0.001, 1016 d.f.). The summary of
324 PRP for peak and trough for theta/high gamma PAC for the odor period are shown for
325 all odorant pairs in Figure 3E (peak PRP) and 3F (trough PRP). For all odorant pairs

326 peak PRP increases for S+ over learning and decreases for S-. Trough PRP is weaker
327 yet follows the same trend as the animal learns to discriminate the odorant as peak
328 PRP (GLM p value < 0.001, 6386 d.f. for S+ vs. S-, peak vs. trough, naïve vs.
329 proficient). In addition, the learning-induced changes in PRP are larger for Exp2 (GLM p
330 value < 0.001 for experiment, 6386 d.f.). Similar changes were found for PRP for
331 theta/beta PAC, but there was no difference between peak and trough (not shown).
332
333 Finally, we found that theta peak phase-referenced power decreases for S- and
334 increases for S+ regardless of the chemical identity of the odorant. Figure 4A shows
335 that after the valence of the odorant is reversed the animal learns to respond to the new
336 rewarded odorant. We asked the question whether odorant-induced changes in peak
337 PRP would change when odorant valence was reversed. Figures 4B and C show that in
338 proficient mice peak PRP increases when the mouse responds to the rewarded odorant
339 regardless of the chemical identity of the odorant, and PRP decreases when the mouse
340 responds to the unrewarded odorant. GLM analysis yields significant changes for
341 odorant, reversal and the interaction of reversal and odorant (p<0.001, 1051 d.f.). These
342 data show that as the animal learns to differentiate between odorants in the go-no go
343 task there is an increase in rewarded odorant-induced peak PRP and a decrease in
344 unrewarded-odorant peak PRP.
345
346 **Linear discriminant analysis classifies stimuli using PRP**
347 The finding that LFP power referenced to the peak of the theta oscillation
348 increases for S+ and decreases for S- when the animal learns to differentiate the odors

349 (naïve vs. proficient) raises the question whether a downstream reader evaluating peak
350 power could decode which stimulus is presented. To assess decoding of olfactory
351 stimuli using PRP, a linear discriminant analysis (LDA) was used to set a decision
352 boundary hyper-plane between binary stimulus classes (S+ versus S-) (Vizcay et al.,
353 2015) using PRP data referenced to the peak (or the trough) of theta/beta or theta/high
354 gamma PAC. LDA was trained with PRP from each electrode for each mouse (16
355 electrodes per mouse) for all trials except one (the training dataset) and then the
356 missing trial (test data) was classified as S+ or S- using the PRP data from that trial.
357 This was performed separately for trials where the mouse was naïve or proficient to
358 odorant discrimination, for each 0.1 sec time point throughout the trial and was repeated
359 for all trials. As a control we shuffled the identity of trials in the training set. In addition,
360 we performed a complementary principal component analysis (PCA) of the PRP to
361 visualize the odor-induced divergence in the time course of the first principal component
362 (PC1).
363
364 Figure 5A shows for theta/beta (i and ii) and theta/high gamma (iii and iv) the
365 time course for PC1 calculated for S+ and S- odorants for naïve (i and iii) and proficient
366 (ii and iv) mice calculated with the PRP for 16 electrodes for one example odorant pair
367 (APEBexp1). In the naïve state PC1 diverged between S+ and S- shortly after water
368 reinforcement for peak and trough theta/beta PRP (Figure 5Ai) and for peak theta/high
369 gamma PRP (Figure 5Aiii, with a smaller change for trough). However, when the animal
370 became proficient PC1 diverged between S+ and S- shortly after odorant addition for
371 theta/beta PRP (Figure 5Aii) and theta/high gamma PRP (Figure 5Aiv). This analysis

372 suggests that for the proficient animal PRP LFP carries information on the rewarded
373 odorant.
374
375 In order to quantify the accuracy for decoding odorant identity using PRP LFP we
376 performed LDA analysis (Figure 5B). For naïve animals the LDA could not classify
377 stimulus identity using peak or trough PRP for either theta/beta (Figure 5Bi) or
378 theta/high gamma (Figure 5Biii). In contrast, when the animal was proficient the
379 precision of the LDA classifier increased shortly after odorant application from chance to
380 values above 70%, significantly higher than the 95% confidence interval of the LDA
381 performed with shuffled trials for both theta/beta (Figure 5Bii) and theta/gamma (Figure
382 5Biv)(GLM analysis p value for learning < 0.001, 104 d.f.). For theta/beta, both peak and
383 trough PRP LDA performed significantly better than shuffled data for proficient mice
384 (Figure 5Bii, GLM p value < 0.001, 104 d.f.). However, for theta/high gamma in
385 proficient animals (Figure 5Biv, bottom) LDA discriminated the identity of the stimulus
386 more effectively using peak PRP (GLM p value < 0.001, 104 d.f.).
387
388 The difference in LDA performance between peak and trough PRP was further
389 evaluated by calculating the area under the curve (AUC) for LDA performance during
390 the odor application window (0.5-2.5 sec after odorant valve opening). AUC is a
391 statistical method to quantify differences between the distributions of values of two
392 variables (Green and Swets, 1988). The AUC was normalized and it ranged from zero
393 (random decoding at 50%, Figure 5-figure supplement 1 Ai) to 1 (100% decoding during
394 the odor period, Figure 5-figure supplement 1 Aii). AUC is plotted for all odorant pairs

395 for peak and trough PRP in Figure 5C for theta/beta (i and ii) and theta/high gamma (iii
396 and iv) for naïve (i,iii) and proficient (ii,iv) conditions. In the proficient state, AUC for
397 peak PRP LDA for high gamma was significantly higher than AUC for trough PRP LDA
398 (Figure 5Civ, GLM for AUC peak vs. trough p value < 0.001, 104 d.f.). AUC for beta
399 PRP LDA did not differ between peak and trough (Figure 5Cii). Furthermore, Figure 5D
400 shows that the AUC was larger for Exp2 (GLM p value < 0.001 for experiment, 6386
401 d.f.).
402
403 Finally, we asked the question whether decoding performance differs when mice
404 make mistakes in the go-no go task. If PRP encodes for the chemical identity of the
405 odorant we would expect that decoding performance would be similar between Hit/Miss
406 and CR/FA during the first second of the trial when the animal keeps their head in the
407 odor port. If PRP encodes for contextual odorant identity decoding performance would
408 differ between correct responses (Hit and CR) and mistakes (Miss, FA) shortly after the
409 animal detects the odorant. Figure 5E shows the results of the per trial analysis of
410 decoding performance for LDA with theta/beta PRP (i) and theta/high gamma PRP (ii)
411 sorted by behavioral outcome. Interestingly, shortly after addition of the odorant there is
412 a divergence in decoding performance between trials with correct decision (Hit, CR) and
413 mistakes (Miss, FA). Shortly after addition of the odorant decoding performance for FA
414 drops below 50% (it tends to encode for the opposite odor), and for Miss trials the
415 decoder performs like the shuffled trials. Decoder performance increases above 50% for
416 both FA and Miss towards the end of the trial. Taken together with the shift of PRP in
417 the reversal experiments (Figure 4) the difference in LDA encoding between correct

trials and mistakes is further evidence that PRP encodes for the contextual identity of the odorant (as opposed to the chemical identity). A GLM analysis indicates that there are significant differences between all behavioral outcomes except for Hit vs. CR for theta/high gamma ($p<0.001$ for all outcome pairs, except for Hit vs CR for theta/beta PRP that has $p<0.01$ and Hit vs. CR for theta/high gamma that has $p>0.05$, 2110 d.f.). There is no significant difference between experiments (GLM $p>0.05$, 2110 d.f.).

To our knowledge, this is the first demonstration of high gamma phase-referenced LFP power developing differential information carrying capacity in early sensory systems with learning.

Decision-making takes place at the same time for peak PRP LDA and licks

After learning that using peak PRP LDA can decode stimulus identity, we wondered how decision-making times estimated based on either the behavioral response of the animal in the go-no go task (licks) or classification of the stimulus by PRP LDA relate to each other. In addition, we asked whether the decision-making time calculated with peak PRP LDA differed from decision-making time estimated using trough PRP LDA. Decision-making time was defined as the time when there is a statistically significant difference between S+ and S- in odorant classification (estimated separately for licks and LDA).

Figures 6A-B show examples of licks by a mouse in the go-no go task for the EAPAexp2 odorant pair. Figure 6A shows the licks detected at the waterspout for 25 S+

441 trials when the animal was performing proficiently while Figure 6B shows the lick traces
442 for 25 S- trials in the same session. As in previous studies (Doucette and Restrepo,
443 2008), we estimated the p value for lick decision-making by computing in each 0.1 sec
444 time bin the ranksum test for the difference between licks (scored 0 for no lick vs. 1 for
445 lick). An example of the time course of the p value for licks for mice performing the go-
446 no go task for EAPAexp2 is shown by the green line in Figure 6Ci. The p value drops
447 below 0.05 ~250 msec after odorant addition. We defined the lick decision-making time
448 as the time point when the p value for difference in licks between S+ and S- falls and
449 stays below 0.05 after odor application.
450
451 LDA decision-making time was estimated in a similar manner by computing the p
452 value for a ranksum test for the difference between predictions (scored 1 for correct
453 prediction vs. 0 for incorrect prediction) for PRP LDA decisions evaluated after pooling
454 data for all mice for each odor pair. As explained under supplemental information
455 (Figure 6-figure supplement 1) pooled animal data was used as opposed to per animal
456 PRP LDA because this resulted in consistent estimation of earlier decision-making
457 times. Examples of the time courses of the p values for PRP LDA performing the go-no
458 go task for EAPAexp2 are displayed in Figure 6Ci for theta/high gamma PAC (red line:
459 peak, blue line: trough). Before odorant presentation the p value fluctuates and
460 sometimes falls below 0.05 transiently, while after odor presentation the p values for
461 peak PRP fall below 0.05 sharply and continuously at approximately the same time as
462 lick p value (~250 msec). Trough PRP p value for LDA decoding performance drops
463 below 0.05 later (~950 msec) and the p values are higher than peak p values (compare

red and blue lines in Figure 6Ci). Thus, in this example lick decision-making time is similar for licks and peak PRP LDA, and is slower for trough PRP LDA.

We proceeded to calculate decision-making times for licks and peak PRP LDA for all odorant pairs. Decision-making times for LDA decoding performance via peak PRP and lick for all odorant pairs for pooled mouse data are shown in Figure 6D for naïve (Figure 6Di) an proficient (Figure 6Dii) mice. Decision times were reduced significantly with task learning (GLM p value < 0.001, 44 d.f.). However, decision-making times did not differ between lick and peak PRP LDA (GLM p value > 0.05, 44 d.f.).

Dimensionality of PRP LFP space decreases when the animal learns to discriminate the odorants

Figure 7A shows the change in the scatter pattern of the first two principal components (PCs) of the theta/high gamma peak PRP calculated for pooled data from all mice as the animals learn to differentiate the two odorants for the EAPAexp1 odorant pair. Figure 7Ai shows that when the mice are naïve S+ (red) and S- (blue) points are mixed in the 2D PC space before and during odorant application. In contrast, Figure 7Aii shows that the 2D PC patterns become clearly separable when the animals are proficient. There appears to be a change in the geometrical arrangement of the points in principal component space suggesting that there is a change in dimensionality as the animal learns to differentiate the odorants (Litwin-Kumar et al., 2017).

487 In order to provide a more nuanced analysis of whether the number of
488 independent signals in the PRP LFP data measured by the 16 electrodes changes as
489 the animals learn to discriminate between odorants we calculated a quantitative
490 measure that characterizes dimensionality in the PRP LFP space (see Methods). The
491 16 electrodes are closely spaced (12.5 μm diameter electrodes in the same tetrode are
492 directly abutted against each other and tetrodes are separated by 100-200 μm in both
493 preparations: Exp1 with optetrodes and Exp2 with tetrodes). Because of this close
494 proximity the extracellular field potentials would not be expected to differ greatly (Gold
495 et al., 2006) and therefore the dimensionality of the PRP LFP space would be expected
496 to be close to one. Interestingly, when the dimensionality was calculated on a per
497 mouse basis where the maximum dimensionality (M) is 16 we found that the average
498 dimensionality for theta/high gamma PRP LFP for electrodes in Exp2 was indeed close
499 to one, but it was significantly higher (2-4) in Exp1, with the highest dimensionality for
500 PRP LFP trough (Figure 7-figure supplement 1 Ai, GLM p value < 0.001 for peak vs.
501 trough and Exp1 vs. Exp2, 379 d.f.). We found similar differences in dimensionality
502 between Exp1 and Exp2 for theta/beta PRP LFP, but in this case there was no
503 difference between peak and trough dimensionality (Figure 7-figure supplement 1 Aii,
504 GLM p value < 0.001 for Exp1 vs. Exp2 and >0.05 for peak vs. trough, 379 d.f.). This
505 indicates that even when measured using electrodes located within 100-200 μm the
506 LFP carries information on multiple independent components.
507
508 Interestingly, the dimensionality for peak PRP LFP for theta/high gamma
509 calculated on a per mouse basis decreased after addition of the odorant for both

experiments and the decrease in dimensionality was larger for proficient mice. Examples of the dimensionality time course for peak PRP LFP for theta/high gamma calculated on a per mouse basis are shown for two odorant pairs in Figure 7-figure supplement 1 Bi (Exp1) and Figure 7-figure supplement 1 Bii (Exp2). A GLM analysis of the dimensionality for peak PRP LFP calculated on a per mouse basis for all odorant pairs indicates that there are significant differences in theta/high gamma peak PRP LFP dimensionality for proficient vs. naïve, time course, experiments, and for interactions of these factors (except for the interaction of experiments x proficient vs. naïve) (GLM p values < 0.001, 6098 d.f.). For theta/beta peak PRP LFP dimensionality we found similar results with the exception that there was no difference between peak and trough (Figure 7-figure supplement 1 Ci and Cii, GLM p values < 0.001, 6098 d.f.).

Finally, when the dimensionality for peak PRP LFP was calculated for LFPs recorded from all mice the difference in the decrease in dimensionality between naïve and proficient became more evident. Time courses for pooled mouse peak PRP LFP dimensionality for theta/high gamma are shown in Figure 7B for Exp1 (7Bi) and Exp2 (7Bii). Peak theta/high gamma PRP LFP dimensionality decreases markedly when the odorant is delivered for both Exp1 and Exp2 for proficient mice and this decrease is larger for proficient compared to naïve mice (compare naïve vs. proficient in Figures 7Bi and ii). A GLM analysis indicates that there are significant differences for time course, proficient vs. naïve, experiments and peak vs. trough, and for interactions of these factors (GLM p values < 0.001, 1688 d.f.). For theta/beta peak PRP LFP dimensionality for pooled mice we found similar results (Figures 7Ci and 7Cii), but there was no

533 difference between peak and trough. GLM analysis found statistically significant
534 differences for time course, and proficient vs. naïve, and for interaction of these factors
535 (GLM p values < 0.001, 1688 d.f.), and a statistically significant difference between
536 experiments (GLM p value < 0.01, 1688 d.f.). However, was no difference between peak
537 and trough (GLM p value >0.05, 1688 d.f). Therefore, for both the per animal and the
538 pooled animal PRP LFP space there is a decrease in dimensionality as the animal
539 learns to discriminate between odorants, but this difference is more evident for the
540 pooled animal data. This is evidence for a learned tightening of dimensionality for the
541 odor representation manifold (defined as the independent neural components
542 representing the odor).
543

Discussion

We asked whether information carried by high frequency oscillations in brain regions involved in early sensory processing changes when observed at different phases of theta frequency oscillations. Specifically, we asked whether information on contextual odorant identity conveyed by LFP power of high gamma and beta frequency oscillations of the OB differs when the downstream observer filters the input through different theta LFP phase windows. We focused on the OB where it has been suggested that amplitude modulation may be used by higher-order processing centers such as PC to decode stimulus identity (Freeman and Schneider, 1982; Heck et al., 2019). We found that identity could not be decoded from beta or high gamma OB LFP power when the mouse was naïve to the identity of the reinforced odorant (left panels in Figure 5B). However, the contextual identity of the odorant could be decoded from the PRP after the animal learned to discriminate between the odorants (right panels in Figure 5B). Furthermore, decoding was more accurate when the high gamma LFP power was observed at the peak of the theta oscillation, but it was similar at both the peak and trough phases for beta LFP oscillations. LDA correctly identified the stimulus with a time course for decision-making similar to the behavioral readout (licking on the water-delivery spout, Figure 6). Thus, stimulus representation by theta phase-referenced beta and high gamma oscillations of the OB evolves over the course of learning. Importantly, our findings were replicated in two different experiments (Exp1 and Exp2) differing in genotype, electrode location, device implanted (tetrode or electrode) and odorant pairs used (see Table S1). We did find differences in measured parameters between experiments, and these are likely due to methodological

differences between Exp1 and Exp2 such as electrode location and genotype. Regardless of the reason for differences between experiments it is important for this study that the findings on PRP are found for both experiments under substantially different experimental conditions. To our knowledge this is the first demonstration that decoding of stimulus identity from theta phase-referenced high gamma oscillations, reflecting synchronized neuronal firing, changes with learning in brain areas involved in early sensory processing.

The importance of PAC in information processing is based on the notion that different information is carried at different phases of the slow carrier oscillation. This discretization of information is a potential mechanism for encoding short-term memories (Lisman and Idiart, 1995) and more broadly as a neural communication protocol, the theta-gamma neural code (Hopfield, 1995; Lisman and Jensen, 2013). Circuit activation at theta frequency was discovered to be essential for long-term potentiation in the rabbit hippocampus (Bliss and Lomo, 1973), arguing that neural information transfer may go beyond mean rate codes and involve spike timing with respect to oscillatory timekeepers. Subsequent studies indicated that temporal windows set by theta cycles allow for local circuit interactions and a considerable degree of computational independence in subdivisions of the entorhinal cortex-hippocampal loop (Mizuseki et al., 2009). For CA1, it was hypothesized that theta partitions the encoding of new information versus the retrieval of stored information (Hasselmo et al., 2002). Indeed, optogenetic recruitment of fast spiking inhibition in CA1 delivered at specific theta phases altered murine performance in a spatial navigation task (Siegle and Wilson,

590 2014). When the mice were encoding a location, triggering of inhibition of CA1 at theta
591 peaks improved performance, whereas inhibition at theta troughs improved
592 performance during the retrieval phase. Recently, age related cognitive decline in
593 working memory in humans was reversed temporarily via transcranial alternating-
594 current stimulation frequency-tuned to the endogenous theta peak frequency of each
595 individual's frontotemporal network (Reinhart and Nguyen, 2019). It appears that
596 working memory is undergirded by theta-gamma PAC and that inter-regional
597 communication is facilitated by theta phase coherence (Daume et al., 2017; Reinhart
598 and Nguyen, 2019). Thus, the theta LFP which has been cited as one of the most global
599 oscillations in the brain acts as a timekeeper (Siegle and Wilson, 2014) that is coherent
600 across numerous cortical and subcortical structures arguing for its role in transfer of
601 discrete chunks of information (Buzsaki, 2002).
602
603 Here we asked whether odor identity information was carried at different phases
604 of theta. Our study of PAC in the OB involved learning of odor discrimination in the go
605 no-go task. In orbitofrontal cortex, Van Wingerden et al. (van Wingerden et al., 2014)
606 showed that this task elicited strongest theta/gamma PAC during odor sampling
607 preceding correct decision-making, which they attributed to temporal coordination
608 between cell assemblies responsible for stimulus representation and reward
609 association. The OB circuit is characterized by beta and gamma oscillations nested in a
610 slower theta carrier wave pertaining to respiration (Buonviso et al., 2003; Heck et al.,
611 2019; Kay, 2005; Kepecs et al., 2006; Rebello et al., 2014; Rojas-Libano et al., 2014).
612 However, Granger directionality analysis shows that the theta oscillation in the OB is

613 also influenced by hippocampal slow oscillations indicating that the origin of OB slow
614 carrier oscillations is complex, involving both respiration and centrifugal input from
615 downstream brain regions whose relative contribution likely changes under different
616 behavioral states (Nguyen Chi et al., 2016). Cyclical activation of OSNs through
617 respiration (Adrian, 1950; Bressler, 1988; Rosero and Aylwin, 2011; Zhuang et al.,
618 2019) provides input to mitral/tufted (M/T) cells, and coordinated activity by M/T cells in
619 the OB caused by mitral cell-granule cell reciprocal dendrodendritic interactions
620 establishes gamma oscillations (Arnson and Strowbridge, 2017; Osinski and Kay, 2016;
621 Pouille and Schoppa, 2018; Schoppa, 2006; Stopfer et al., 1997)(see review by (Heck
622 et al., 2019)). Gamma LFP is thought to represent the stimulus identity (Bathellier et al.,
623 2006; Beshel et al., 2007; Li and Cleland, 2017; Rojas-Libano and Kay, 2008) and beta
624 LFP oscillations (15-35 Hz) have been linked to learned reward (Martin et al., 2006).
625 However, the classification of these two bandwidths as carrying learning vs. odor
626 identity information is not always appropriate, and Frederick et al. (Frederick et al.,
627 2016) proposed that they represent different cognitive states that vary depending on
628 particular behavioral demands. PAC is present in the OB (Buonviso et al., 2003; Rojas-
629 Libano et al., 2014) and it may be of great albeit relatively unexplored utility. We
630 contributed to the understanding of which information is carried by different frequency
631 oscillations by asking whether the high gamma and beta oscillations carry different
632 information when they are observed within particular phase windows of the theta carrier
633 wave (Figure 5). We hypothesized that PAC may be used to convey olfactory stimulus
634 information to theta phase-synchronized downstream regions like PC (Kepecs et al.,
635 2006; Lisman and Buzsaki, 2008).

636

637 We demonstrate that PAC changes in the OB during associative learning (Figure
638 2). Peak angle variance increased for the unrewarded odorants with learning. The theta
639 phase-referenced PRP of the high gamma and beta LFPs also follows this trend (Figure
640 3), increasing for S+ and decreasing with S- over learning. The changes in PRP
641 correlating with learning may reflect contrast enhancement that facilitates the
642 discrimination between similar stimuli by a downstream observer. Neuronal adaptation
643 to facilitate contrast enhancement has been shown at the level of the OSNs (Haney et
644 al., 2018), the glomerular layer (Cavarretta et al., 2016), and the granule cell layer
645 (Adams et al., 2019) of the OB. We speculate that the concurrent increase in PRP for
646 S+ and decrease in PRP for S- reflects adaptational mechanisms in the OB to enhance
647 contrast between similar stimuli with different associated values.

648

649 To quantify whether these changes in PAC increased discriminability between
650 odorants using PRP we asked whether the stimulus that was delivered could be
651 decoded from PRP data. Previous investigations have decoded olfactory stimuli from
652 spike counts aligned to sniffing in the mouse (Cury and Uchida, 2010; Gschwend et al.,
653 2012), in the antennal lobe of the locust (Stopfer and Laurent, 1999), and M/T neural
654 activity assayed through calcium transients in mice (Chu et al., 2016), but trial
655 classification via PAC remains unexplored. Here, we performed LDA on PRP data to
656 determine whether a single hyperplane could differentiate between stimuli as the
657 animals learned the task. Figure 5B indicates that the identity of the stimuli cannot be
658 decoded from PRP recorded in the naïve mice, but that the stimuli can be decoded

659 when the mice learn to discriminate the odorants. Furthermore, decoding the stimuli
660 from peak high gamma PRP is significantly better than trough PRP. Thus, decoding of
661 the odorant identity by downstream observer using a phase window for the slow carrier
662 oscillation could detect the identity of the odorants after the animal learns to differentiate
663 between odors in the go no-go task. Finally, this study contributes to the mounting
664 evidence that the OB is an important locus for learning-related activity changes
665 (Abraham et al., 2014; Doucette et al., 2011; Doucette and Restrepo, 2008; Koldaeva et
666 al., 2019; Li et al., 2015).
667
668 We wondered how timing for decision-making would relate comparing stimulus
669 decoding with PRP with decision-making estimated from the behavioral readout of the
670 olfactory-driven decision in the go no-go task (differential licking between the two
671 odorants). The time course for the behavioral decision, reflected in the graph of p value
672 for differential licks, is overlaid by the p value time course for peak PRP decoding
673 (Figure 6C, right) with trough PRP lagging behind. Neither beta nor high gamma peak
674 PRP p values are discriminable from lick p values in terms of decision time in this task.
675 As shown in Figure 6D, for proficient animals licking differs between odorants within
676 about 0.5 seconds from stimulus onset, at the same time that PRP decoding becomes
677 significant. This is slower than discrimination times for odorant responses recorded in
678 mice performing two alternative forced choice odorant discrimination or receiving odors
679 passively where discrimination takes place within the first respiratory cycle (~250 ms)
680 after stimulus onset (Cury and Uchida, 2010; Short and Wachowiak, 2019; Shusterman
681 et al., 2011). However, the 0.5 sec decision-making time is consistent with studies with

682 the go no-go task where there is not a strong motivation for the animal to stop licking for
683 the unrewarded odorant (Abraham et al., 2004; Doucette and Restrepo, 2008; Jordan et
684 al., 2018; Rinberg et al., 2006)—with the exception of rapid detection of optogenetic
685 activation of glomerular input in the go no-go task (Smear et al., 2011). Thus, we
686 conclude that PRP is an accurate reflection of decision-making in olfactory
687 discrimination.
688
689 Interestingly, in contrast with theta/high gamma PRP where the decoding
690 performance for peak and through differ substantially, for theta/beta PRP there is no
691 difference in decoding performance between peak and trough (compare Figures 5Bii
692 and 5Biv). Increases in OB beta LFP for rodents engaged in odorant discrimination
693 tasks take place after the onset of changes in gamma LFP and it has been postulated
694 that beta LFP represents systemwide coherent states perhaps conveying centrifugal
695 modulation from downstream brain areas to the OB (David et al., 2015; Frederick et al.,
696 2016; Kay, 2014). If beta oscillations indeed represent centrifugal feedback our findings
697 suggest that centrifugal modulation does not differ through phases of the theta
698 oscillation and would therefore excerpt modulation on high frequency circuit activity
699 occurring at different theta phases. Here we show that peak-referenced high gamma
700 oscillation power encodes for the contextual identity of the odorant (is the odorant
701 rewarded?). What information could be conveyed at other theta phases is an open
702 question. Perhaps asynchronous M/T firing carries chemical odorant information in the
703 theta trough.
704

705 Finally, we turn to dimensionality. The measurements in the experiments
706 presented here are inherently low dimensional because: 1) The animal is discriminating
707 between two odors, and the behavior is constrained by the go no-go task (Gao et al.,
708 2017) and 2) While the number of independent degrees of freedom for inputs to the OB
709 is potentially large (~2000 glomeruli), the four tetrodes are close together and they
710 should sample a small subset of these input dimensions. Indeed, because the tetrodes
711 are within 200 μm of each other (and electrodes are adjacent within tetrodes), the LFP
712 recorded from each electrode is likely to be similar, assuming that the cellular milieu
713 around the electrodes does not separate the inputs (Gold et al., 2006). Interestingly, the
714 dimensionality measured from the 16 electrodes (four tetrodes) varies between 1 and 6
715 suggesting that subsets of electrodes are detecting different signals (Figure 7-figure
716 supplement 1 A). However, when the mice learn to discriminate the dimensionality
717 decreases in the presence of the relevant odorant (Figures 7 and Figure 7-figure
718 supplement 1 B and C), suggesting that population representation is a modifiable
719 aspect of OB processing. This likely reflects experience-dependent, attention (Canas
720 and Jones, 2010; Niv et al., 2015). In the naïve state, relevant (rewarded) dimensions
721 are unknown to the mouse, and a downstream structure sampling from the recorded
722 population would receive ambiguous signaling in the presence of the rewarded odorant
723 without decoding or reducing the input information. We find a large decrease in
724 dimensionality post-learning, suggesting that OB now enhances a relevant and invariant
725 signal to allow for unambiguous odor detection. Attention, guided by reward prediction
726 error, likely biases/constrains the learning to the relevant dimensions (Leong et al.,
727 2017)—in this task, odor identity.

The changes in signal processing elicited by learning, habituation, and passive odorant exposure in the OB, the earliest processing center in the olfactory system, are remarkable. Why is processing in this circuit so plastic and influenced by centrifugal input from downstream targets, such as PC, and from a variety of neuromodulatory centers (Gire et al., 2013b; Linster and Cleland, 2016)? Likely the reason is that this processing center receives massive parallel glomerular input and projects M/T output of high dimensionality to downstream brain processing areas (Chae et al., 2019). Furthermore, unsupervised learning modifying cellular interactions in the OB would increase dimensionality (Hiratani and Latham, 2019). Therefore, odors must be identified in the midst of a high dimensionality cocktail party (Rokni et al., 2014). Based on the present data showing a large increase in the accuracy for decoding of contextual odor identity from the PRP as the animal learns to differentiate the odorants we speculate that when a subset of the degrees of freedom of the sensory input become behaviorally relevant, centrifugal feedback elicits supervised learning that results in a decrease in dimensionality of the output from the OB to downstream brain areas. Thus, the fact that peak theta-referenced high gamma power encodes information on whether the odorant is rewarded may simply reflect the fact that the transfer of sensory information on the rewarded odorant is being prioritized in the OB circuit. This would result in more accurate discrimination of the input channels that are relevant to the current task. Whether (and how) supervised learning-induced OB circuit plasticity results in a decrease in dimensionality of the output remains to be determined.

751 **Materials and Methods**

752 **Key Resources Table**

REAGENT TYPE	REAGENT or RESOURCE	SOURCE	IDENTIFIER	ADDITIONAL INFORMATION
Chemical compound, drug	Isoamyl acetate	Sigma-Aldrich	Cat#123-92-2	Odorant
Chemical compound, drug	Ethyl acetate	Sigma-Aldrich	Cat# 141-78-6	Odorant
Chemical compound, drug	Propyl acetate	Sigma-Aldrich	Cat# 109-60-4	Odorant
Chemical compound, drug	Mineral oil	Sigma-Aldrich	Cat# 8042-47-5	Odorant
Chemical compound, drug	Acetophenone	Sigma-Aldrich	Cat# 98-86-2	Odorant
Chemical compound, drug	Ethyl benzoate	Sigma-Aldrich	Cat# 93-89-0	Odorant
Other	Nickel-chrome wire	Sandvik	Cat#PX000002	Tetrode fabrication
Other	16 Channel Electrode Interface Board	Neuralynx	EIB-16	Tetrode fabrication
Software, algorithm	Analysis code	This paper	Available on github and by request	https://github.com/restrepd/drgMaster
Strain, strain background	Mouse: C57BL/6J	Jackson Lab	RRID: IMSR_JAX:000664	Male mice
Strain, strain background	Mouse: Tg(Dbh-cre)KH212Gsat/Mmucd	Mutant Mouse Resource and Research Center	032081-UCD, RRID:MMRRC	All sexes used
Strain, strain background	Mouse: eNpHR3.0, 129S-Gt(ROSA)26Sortm39(CAG-hop/EYFP) Hze/J	Jackson Lab	014539, RRID:SCR_004633	All sexes used
Software, algorithm	MATLAB_R2018a	Mathworks	RRID: SCR_001622	
Software, algorithm	Illustrator	Adobe	RRID: SCR_010279	
Software, algorithm	Photoshop	Adobe	RRID: SCR_014199	

753

754 *Animals*

755 The study was performed in two sets of experiments. For the first set of
756 experiments (Exp1), DBH-eNpHR3.0 mice were used as per Ramirez-Gordillo et al.,
757 2018. These mice express halorhodopsin in cells expressing Cre under the *Dbh*
758 promoter (DBH-Cre eNpHR3.0) in LC-NA neurons and were produced by crossing
759 DBH-Cre mice (032081-UCD, Mutant Mouse Resource and Research Center) with
760 mice expressing halorhodopsin in a Cre-dependent fashion [eNpHR3.0,
761 129S Gt(ROSA)26Sortm39(CAG-hop/EYFP) Hze/J, Jackson labs]. C57BL/6 mice
762 (Jackson stock number: 000664) were used for the second set of experiments (Exp2).
763 All animal procedures were performed under approval from the Institutional Animal Care
764 and Use Committee (IACUC) at the University of Colorado Anschutz Medical Campus
765 under guidelines from the National Institutes of Health. The number of mice used in
766 each experiment is shown in Table S1.

767

768 *(Op)tetrode implantation*

769 Surgery was performed under approval from the Institutional Animal Care and
770 Use Committee (IACUC) at the University of Colorado Anschutz Medical Campus, using
771 aseptic technique. As per Li et al. (2015), tetrode boards (EIB-16, Neuralynx) with
772 optional fiber optic cannula for photostimulation (optetrodes) were populated with four
773 tetrodes consisting of four 12.5 μm nichrome wires coated with polyimide (Sandvik
774 RO800). For optetrode fabrication the tetrode boards received the addition of a fiber
775 optic cannula 105 μm in diameter (Thorlabs FG105UCA) with 1.25 mm OD ceramic
776 ferrule (Precision Fiber Products) for coupling to a DPSS laser (473 nm, Shanghai

777 Laser and Optics Century). The optogenetic experiments of Ramirez-Gordillo et al.
778 (2018) are not included in this study. In the rest of the text we refer to the inserts as
779 (op)tetrode with the understanding that optetrodes were implanted for Exp1 while
780 tetrodes were implanted for Exp2. Electrode tips were electroplated to 0.2-0.4 MΩ
781 impedance.
782
783 Two-month-old male mice were anesthetized with 5% isoflurane in oxygen.
784 Intraperitoneal ketamine/xylazine (100 mg/kg and 10 mg/kg respectively) was then
785 administered along with 100 µl of 2% lidocaine injected subcutaneously over the skull.
786 After the mouse was found to be unresponsive to a toe pinch, the animal's head was
787 then secured in the stereotaxic apparatus (Narishige SR-5M-HT) and the skull was
788 leveled (≤ 50 µm difference DV between bregma and lambda). Gentamycin ophthalmic
789 ointment was applied to the eyes to maintain hydration. After incising the skin overlaying
790 the skull, the periosteum was cleared with 15% H_2O_2. A manipulator (Sutter MP-285)
791 was zeroed at bregma and midline and the target location for OB implantation was
792 marked with respect to bregma (Exp1: AP +4.28 mm, ML +0.4 mm, Exp2: AP +4.28
793 mm, ML +0.5 mm).
794
795 A craniotomy performed at this site (Marathon III drill) exposed dura mater which
796 was removed prior to implantation. Another craniotomy was performed more caudally
797 for implantation of one ground screw (Plastics1 00-96 x 1/16). The (op)tetrode was
798 positioned above the craniotomy over the OB while the ground wire was wrapped
799 around the ground screw with the connection coated in silver paint (SPI Flash-Dry silver

conductive paint). After securing the ground screw to the skull, the (op)tetrodes were lowered into position at the rate of 1 mm/minute (Exp1: AP +4.28 mm, ML +0.4 mm, DV 0.53 mm, Exp2: AP +4.28 mm, ML +0.5 mm, DV 1.0 mm). After reaching the target depth, the optetrode was adhered to the skull with C&B Metabond, followed by Teets 'Cold Cure' dental cement. After curing (10 minutes), the (op)tetrode was detached from the manipulator, the animal was removed from the stereotax and received subcutaneous injections of carprofen (10 mg/kg) and buprenorphine (0.05 mg/kg) and recovered on a heating pad kept at 37°C. The mice were monitored daily and received additional carprofen injections daily for the first two days postoperatively.

Go-no go behavioral task

Mice were water deprived until they reached 80% normal body mass. Then they were placed into the Slotnick olfactometer (Bodyak and Slotnick, 1999; Li et al., 2015) chamber where they could move freely. All mice were first trained to lick the water spout to obtain water in the presence of odor (1% isoamyl acetate in mineral oil, v/v) in the "begin" task (Slotnick and Restrepo, 2005). Subsequently they learned to discriminate 1% isoamyl acetate (S+) versus mineral oil (S-) in the "go no-go" task (Doucette et al., 2011; Li et al., 2015), followed by learning to discriminate other odorant pairs (Table S1). Data were analyzed for the go-no go discrimination task, but not for the begin task.

Mice self-initiated trials by poking their head into the odor delivery port, breaking a photodiode beam (Figure 1A). During reinforced odorant delivery (lasting 2.5 seconds) they must lick a water delivery spout at least once during each of four 0.5 second-long

823 response areas in order to register the decision as a Hit (Figure 1B). Licks were
824 detected as electrical connectivity between the water spout and the ground plate on
825 which they stand (Slotnick and Restrepo, 2005). If the mice licked during a rewarded
826 odorant trial, they received ~10 µl water reinforcement (Figure 1C). The mice learn to
827 refrain from licking for the unrewarded odorant due to the unrewarded effort of
828 sustained licking. For correct rejections mice leave the spout shortly after the last lick
829 that takes place 0.5-1.8 sec after odorant onset (Figure 6B). Performance was
830 evaluated in blocks of 20 trials, with 10 S+ and 10 S- trials presented at random.
831 Animals performed as many as 10 blocks per session. Sessions were terminated when
832 animals demonstrated satiety/disengagement from the task or when they performed at
833 or above 80% correct discrimination in three or more blocks in a session. For
834 EAPAexp1, IAAPexp2 and EAPAexp2 once criterion was reached, the next session had
835 reversed valence, meaning that the previous S+ became S- (and the previous S-
836 became S+). This reversal disambiguates the identity of the odor from its valence. Data
837 were analyzed for all odorant pair sessions, including isoamyl acetate vs. mineral oil.
838 Data were analyzed within two performance windows: when the animal was performing
839 below 65% (naïve) or above 80% (proficient). The data were also analyzed in the 65-
840 80% performing window, and the results fell between the naïve and proficient windows
841 (data not shown).
842
843 Odor stimulus delivery time was measured with a photoionization detector
844 (miniPID, Aurora Scientific). Figure 1-figure supplement 1 shows the time course for
845 odorant concentration measured at the odor spout. The time difference between valve

opening and detection of odor at the odor port was between 66 – 133 ms, depending on which olfactometer was used.

Neural recording

Extracellular potentials from the four tetrodes were captured and digitized at 20 kHz on the RHD2216 amplifier of the Intan RHD2000 Evaluation System with a 1-750 Hz bandpass filter. Information on behavioral events (valve times, mouse presence at the odor port) was sent through a digital line from the Slotnick olfactometer to the Intan board. Licks detected by the Slotnick olfactometer were recorded as an analog signal by the Intan board.

Phase Amplitude Coupling

PAC data were processed using the Hilbert transform method described by Tort *et al.*, 2010. Briefly, data were bandpass filtered with a 20th order Butterworth filter using Matlab's filtfilt function with zero phase shift to extract LFP in the low frequency oscillation used for phase estimation (theta, 2-14 Hz, Figure 1Diii) and the high frequency oscillation used for estimation of the amplitude of the envelope (either beta, 15-30 Hz, or high gamma, 65-95 Hz, Figure 1v). Hilbert transform established the theta phase (Figure 1Div) and, separately, the envelope for beta or high gamma (red line in Figure 1Dv). A plot of the distribution of beta/high gamma amplitude in 51 bins of the phase of theta (PAC) was plotted to gauge the strength of PAC (Figure 1E). To quantify the strength of PAC we calculated the MI estimating the KL distance to quantify the difference between the observed beta/high gamma amplitude distribution along the

869 phase of theta from a uniform distribution. If PAC is non-existent, MI = 0, meaning the
870 mean amplitude is distributed uniformly over theta phases, and if PAC is a delta function
871 MI = 1. MI for signals measured in brain areas such as the hippocampus typically fall
872 between 0-0.03 (Tort et al., 2010).
873
874 *Phase-referenced LFP power*
875 Beyond the mere existence of PAC that has been documented in numerous brain
876 regions, we sought to evaluate whether the information carried by beta or high gamma
877 power at different theta phases could be used to discriminate between olfactory stimuli.
878 To accomplish this analysis, we developed the PRP approach using custom Matlab
879 code. Briefly, PAC was calculated using the approach documented by Tort *et al.*, 2010,
880 as described above and summarized in Figure 1. Peak and trough theta phases are
881 defined as the phase for maxima and minima of the PAC distribution measured for the
882 S+ trials (red plot in Figure 2C). A continuous Morlet wavelet transform was used to
883 estimate the power for the high frequency oscillations (Buonviso et al., 2003). PRP was
884 estimated as the power of the high frequency oscillations (beta or high gamma)
885 measured at the peak or trough of PAC (Figure 5). The Matlab code used for data
886 analysis has been deposited to https://github.com/restrepd/drgMaster.
887
888 *PAC/PRP Simulation*
889 To validate our analysis of PAC and PRP, we performed simulations with
890 uncoupled oscillations (no PAC) with a low frequency cosine oscillation at 8 Hz and a
891 high frequency cosine oscillation at 40 Hz (Figure 1-figure supplement 2A) or with

892 coupled oscillations where high frequency bursts took place at 180 degrees for the low
893 frequency cosine oscillation (Figure 1-figure supplement 2B). The bursts were
894 generated by a cosine oscillation at the high frequency multiplied by gaussians with a
895 full width half maximum of (1/8 Hz)/2 centered at 180 degrees of the low frequency
896 cosine wave. Top panels in both S1A and S1B are pseudocolor Morlet wavelet power
897 time courses, while the bottom panels show the PRP of the 40 Hz oscillation. For the
898 case with no PAC (Figure 1-figure supplement 2A), peak and trough PRP are equal.
899 However, for the PAC example (Figure 1-figure supplement 2B) the peak PRP is
900 significantly higher than trough PRP.
901
902 *Statistical analysis*
903 Statistical analysis was performed in Matlab. PAC parameters and PRP were
904 calculated separately per electrode (16 electrodes per mouse) for all electrodes per
905 mouse. Statistical significance for changes in measured parameters for factors such as
906 learning and odorant identity was estimated using generalized linear model (GLM)
907 analysis, with post-hoc tests for all data pairs corrected for multiple comparisons using
908 false discovery rate (Curran-Everett, 2000). The post hoc comparisons between pairs of
909 data were performed either with a t-test, or a ranksum test, depending on the result of
910 an Anderson-Darling test of normality. GLM is a general statistical method that includes
911 regression and analysis of variance. Degrees of freedom and statistical significance
912 have the same meaning in GLM as in analysis of variance and regression (Agresti,
913 2015). In addition, as a complementary assessment of significant differences (Halsey et
914 al., 2015) we display 95% confidence intervals (CIs) shown in the figures as vertical

black lines were estimated by bootstrap analysis of the mean by sampling with replacement 1000 times.

Linear discriminant analysis

Classification of trials using PRP was accomplished via LDA in Matlab whereby PRP for every trial except one were used to train the LDA, and the missing trial was classified by the LDA prediction. This was repeated for all trials and was performed separately for peak and trough PRP, and for analysis where the identity of the odorants was shuffled. LDA and dimensionality analysis were performed either on a per-mouse basis where the input was the PRP recorded from 16 electrodes, or on pooled mouse data where the input was the PRP recorded from 16 x N electrodes where N is the number of mice. For pooled mouse analysis a pooled response vector was therefore created by concatenating across animals and the number of trials *n*, was determined by the session with the lowest number of trials for a single odorant (Chu et al., 2016).

Dimensionality

Following Litwin-Kumar et al. (2017) we defined the dimension of the system (dim) with *M* inputs as the square of the sum of the eigenvalues of the covariance matrix of the measured PRP LFP (*pLFP*) divided by the sum of each eigenvalue squared:

$$\dim\,(pLFP) = \left(\sum_{i=1}^{M} \lambda_{\mathrm{i}}\right)^{2} / \left(\sum_{i=1}^{M} {\lambda_{\mathrm{i}}}^{2}\right)$$

where λ_i are the eigenvalues of the covariance matrix of *pLFP* computed over the distribution of PRP LFP signals measured in the OB. If the components of *pLFP* are independent and have the same variance, all the eigenvalues are equal and dim(*pLFP*) = *M*. Conversely, if the *pLFP* components are correlated so that the data points are distributed equally in each dimension of an *m*-dimensional subspace of the full *M*-dimensional space, only *m* eigenvalues will be nonzero and dim(*pLFP*) = *m*.

Acknowledgments: We thank Ms. Nicole Arevalo for animal husbandry, Ms. Dnate' Baxter for laboratory support, Dr. Douglas Curran-Everett for advice on statistical analysis, Dr. Cecilia Gauthier Umaña for discussions on wavelet analysis and Ms. Arianna Gentile-Polese for immunohistochemical assays. This research was supported by NIDCD 1F31DC016483-01A1 to J.L. and NIDCD 5R01DC000566-30 to D.R.

Declaration of interests: The authors declare no competing interests.

952 **References**

953

954 Abraham, N.M., Spors, H., Carleton, A., Margrie, T.W., Kuner, T., and Schaefer, A.T.
955 (2004). Maintaining accuracy at the expense of speed: stimulus similarity defines odor
956 discrimination time in mice. Neuron *44*, 865-876.

957 Abraham, N.M., Vincis, R., Lagier, S., Rodriguez, I., and Carleton, A. (2014). Long term
958 functional plasticity of sensory inputs mediated by olfactory learning. Elife *3*, e02109.

959 Adams, W., Graham, J.N., Han, X., and Riecke, H. (2019). Top-down inputs drive
960 neuronal network rewiring and context-enhanced sensory processing in olfaction. PLoS
961 Comput Biol *15*, e1006611.

962 Adrian, E.D. (1950). The electrical activity of the mammalian olfactory bulb.
963 Electroencephalography and Clinical Neurophysiology *2*, 377-388.

964 Agresti, A. (2015). Foundations of linear and generalized linear models. In Wiley series
965 in probability and statistics (Hoboken, New Jersey: John Wiley & Sons Inc.,), pp. 1
966 online resource.

967 Amemiya, S., and Redish, A.D. (2018). Hippocampal Theta-Gamma Coupling Reflects
968 State-Dependent Information Processing in Decision Making. Cell Rep *25*, 3894-3897.

969 Arnson, H.A., and Strowbridge, B.W. (2017). Spatial Structure of Synchronized
970 Inhibition in the Olfactory Bulb. J Neurosci *37*, 10468-10480.

Bathellier, B., Lagier, S., Faure, P., and Lledo, P.M. (2006). Circuit properties generating gamma oscillations in a network model of the olfactory bulb. J Neurophysiol *95*, 2678-2691.

Beshel, J., Kopell, N., and Kay, L.M. (2007). Olfactory bulb gamma oscillations are enhanced with task demands. J Neurosci *27*, 8358-8365.

Bliss, T.V., and Lomo, T. (1973). Long-lasting potentiation of synaptic transmission in the dentate area of the anaesthetized rabbit following stimulation of the perforant path. J Physiol *232*, 331-356.

Bodyak, N., and Slotnick, B. (1999). Performance of mice in an automated olfactometer: odor detection, discrimination and odor memory. ChemSenses *24*, 637-645.

Bragin, A., Jando, G., Nadasdy, Z., Hetke, J., Wise, K., and Buzsaki, G. (1995). Gamma (40-100 Hz) oscillation in the hippocampus of the behaving rat. J Neurosci *15*, 47-60.

Bressler, S.L. (1988). Changes in electrical activity of rabbit olfactory bulb and cortex to conditioned odor stimulation. Behav Neurosci *102*, 740-747.

Buonviso, N., Amat, C., Litaudon, P., Roux, S., Royet, J.P., Farget, V., and Sicard, G. (2003). Rhythm sequence through the olfactory bulb layers during the time window of a respiratory cycle. EurJNeurosci *17*, 1811-1819.

Buzsaki, G. (2002). Theta oscillations in the hippocampus. Neuron *33*, 325-340.

Buzsaki, G. (2010). Neural syntax: cell assemblies, synapsembles, and readers. Neuron *68*, 362-385.

Buzsaki, G., and Draguhn, A. (2004). Neuronal oscillations in cortical networks. Science *304*, 1926-1929.

Canas, F., and Jones, M. (2010). Attention and reinforcement learning: constructing representations from indirect feedback. Paper presented at: Proceedings of the Annual Meeting of the Cognitive Science Society.

Canolty, R.T., and Knight, R.T. (2010). The functional role of cross-frequency coupling. Trends Cogn Sci *14*, 506-515.

Cavarretta, F., Marasco, A., Hines, M.L., Shepherd, G.M., and Migliore, M. (2016). Glomerular and Mitral-Granule Cell Microcircuits Coordinate Temporal and Spatial Information Processing in the Olfactory Bulb. Front Comput Neurosci *10*, 67.

Chae, H., Kepple, D.R., Bast, W.G., Murthy, V.N., Koulakov, A.A., and Albeanu, D.F. (2019). Mosaic representations of odors in the input and output layers of the mouse olfactory bulb. Nat Neurosci *22*, 1306-1317.

Chery, R., Gurden, H., and Martin, C. (2014). Anesthetic regimes modulate the temporal dynamics of local field potential in the mouse olfactory bulb. J Neurophysiol *111*, 908-917.

Chrobak, J.J., and Buzsaki, G. (1998). Gamma oscillations in the entorhinal cortex of the freely behaving rat. J Neurosci *18*, 388-398.

Chu, M.W., Li, W.L., and Komiyama, T. (2016). Balancing the Robustness and Efficiency of Odor Representations during Learning. Neuron *92*, 174-186.

1011 Courtiol, E., and Wilson, D.A. (2017). The Olfactory Mosaic: Bringing an Olfactory
1012 Network Together for Odor Perception. Perception *46*, 320-332.

1013 Curran-Everett, D. (2000). Multiple comparisons: philosophies and illustrations.
1014 AmJPhysiol RegulIntegrComp Physiol *279*, R1-R8.

1015 Cury, K.M., and Uchida, N. (2010). Robust odor coding via inhalation-coupled transient
1016 activity in the mammalian olfactory bulb. Neuron *68*, 570-585.

1017 Daume, J., Gruber, T., Engel, A.K., and Friese, U. (2017). Phase-Amplitude Coupling
1018 and Long-Range Phase Synchronization Reveal Frontotemporal Interactions during
1019 Visual Working Memory. J Neurosci *37*, 313-322.

1020 David, F., Courtiol, E., Buonviso, N., and Fourcaud-Trocme, N. (2015). Competing
1021 Mechanisms of Gamma and Beta Oscillations in the Olfactory Bulb Based on
1022 Multimodal Inhibition of Mitral Cells Over a Respiratory Cycle. eNeuro *2*.

1023 Doucette, W., Gire, D.H., Whitesell, J., Carmean, V., Lucero, M.T., and Restrepo, D.
1024 (2011). Associative cortex features in the first olfactory brain relay station. Neuron *69*,
1025 1176-1187.

1026 Doucette, W., and Restrepo, D. (2008). Profound context-dependent plasticity of mitral
1027 cell responses in olfactory bulb. PLoS Biol *6*, e258.

1028 Engel, A.K., Fries, P., Konig, P., Brecht, M., and Singer, W. (1999). Temporal binding,
1029 binocular rivalry, and consciousness. Conscious Cogn *8*, 128-151.

1030 Florin, E., and Baillet, S. (2015). The brain's resting-state activity is shaped by
1031 synchronized cross-frequency coupling of neural oscillations. Neuroimage *111*, 26-35.

1032 Frederick, D.E., Brown, A., Brim, E., Mehta, N., Vujovic, M., and Kay, L.M. (2016).
1033 Gamma and Beta Oscillations Define a Sequence of Neurocognitive Modes Present in
1034 Odor Processing. J Neurosci *36*, 7750-7767.

1035 Freeman, W.J., and Schneider, W. (1982). Changes in spatial patterns of rabbit
1036 olfactory EEG with conditioning to odors. Psychophysiology *19*, 44-56.

1037 Fries, P. (2005). A mechanism for cognitive dynamics: neuronal communication through
1038 neuronal coherence. Trends Cogn Sci *9*, 474-480.

1039 Gao, P., Trautmann, E., Byron, M.Y., Santhanam, G., Ryu, S., Shenoy, K., and Ganguli,
1040 S. (2017). A theory of multineuronal dimensionality, dynamics and measurement.
1041 BioRxiv, 214262.

1042 Gire, D.H., Kapoor, V., Seminara, A., Arrighi-Allisan, A., and Murthy, V.N. (2013a).
1043 Olfactory search behavior in mice: A novel task design that moves beyond a single sniff.
1044 Society for Neuroscience 2013 Online *Program No. 452.28*.

1045 Gire, D.H., Restrepo, D., Sejnowski, T.J., Greer, C., De Carlos, J.A., and Lopez-
1046 Mascaraque, L. (2013b). Temporal processing in the olfactory system: can we see a
1047 smell? Neuron *78*, 416-432.

1048 Gold, C., Henze, D.A., Koch, C., and Buzsaki, G. (2006). On the origin of the
1049 extracellular action potential waveform: A modeling study. JNeurophysiol *95*, 3113-
1050 3128.

1051 Gourevitch, B., Kay, L.M., and Martin, C. (2010). Directional coupling from the olfactory
1052 bulb to the hippocampus during a go/no-go odor discrimination task. J Neurophysiol
1053 *103*, 2633-2641.

1054 Green, D.M., and Swets, J.A. (1988). Signal detection theory and psychophysics, Vol
1055 Reprint ed (Los Altos, Calif., USA: Peninsula Pub).

1056 Gschwend, O., Beroud, J., and Carleton, A. (2012). Encoding odorant identity by spiking
1057 packets of rate-invariant neurons in awake mice. PloS one *7*, e30155.

1058 Halsey, L.G., Curran-Everett, D., Vowler, S.L., and Drummond, G.B. (2015). The fickle
1059 P value generates irreproducible results. Nature methods *12*, 179-185.

1060 Haney, S., Saha, D., Raman, B., and Bazhenov, M. (2018). Differential effects of
1061 adaptation on odor discrimination. J Neurophysiol *120*, 171-185.

1062 Harno, E., Cottrell, E.C., and White, A. (2013). Metabolic pitfalls of CNS Cre-based
1063 technology. Cell Metab *18*, 21-28.

1064 Hasselmo, M.E., Bodelon, C., and Wyble, B.P. (2002). A proposed function for
1065 hippocampal theta rhythm: separate phases of encoding and retrieval enhance reversal
1066 of prior learning. Neural Comput *14*, 793-817.

Heck, D.H., Kozma, R., and Kay, L.M. (2019). The rhythm of memory: how breathing shapes memory function. J Neurophysiol *122*, 563-571.

Hiratani, N., and Latham, P.E. (2019). Rapid Bayesian learning in the mammalian olfactory system. bioRxiv, 706200.

Hopfield, J.J. (1995). Pattern recognition computation using action potential timing for stimulus representation. Nature *376*, 33-36.

Jensen, O. (2001). Information transfer between rhythmically coupled networks: reading the hippocampal phase code. Neural Comput *13*, 2743-2761.

Jordan, R., Fukunaga, I., Kollo, M., and Schaefer, A.T. (2018). Active Sampling State Dynamically Enhances Olfactory Bulb Odor Representation. Neuron *98*, 1214-1228 e1215.

Kay, L.M. (2005). Theta oscillations and sensorimotor performance. Proc Natl Acad Sci U S A *102*, 3863-3868.

Kay, L.M. (2014). Circuit oscillations in odor perception and memory. Prog Brain Res *208*, 223-251.

Kay, L.M. (2015). Olfactory system oscillations across phyla. Curr Opin Neurobiol *31*, 141-147.

Kepecs, A., Uchida, N., and Mainen, Z.F. (2006). The sniff as a unit of olfactory processing. ChemSenses *31*, 167-179.

1086 Koldaeva, A., Schaefer, A.T., and Fukunaga, I. (2019). Rapid task-dependent tuning of
1087 the mouse olfactory bulb. Elife *8*.

1088 Lega, B., Burke, J., Jacobs, J., and Kahana, M.J. (2016). Slow-Theta-to-Gamma Phase-
1089 Amplitude Coupling in Human Hippocampus Supports the Formation of New Episodic
1090 Memories. Cereb Cortex *26*, 268-278.

1091 Leong, Y.C., Radulescu, A., Daniel, R., DeWoskin, V., and Niv, Y. (2017). Dynamic
1092 Interaction between Reinforcement Learning and Attention in Multidimensional
1093 Environments. Neuron *93*, 451-463.

1094 Li, A., Gire, D.H., and Restrepo, D. (2015). Y spike-field coherence in a population of
1095 olfactory bulb neurons differentiates between odors irrespective of associated outcome.
1096 J Neurosci *35*, 5808-5822.

1097 Li, A., Zhang, L., Liu, M., Gong, L., Liu, Q., and Xu, F. (2012). Effects of different
1098 anesthetics on oscillations in the rat olfactory bulb. J Am Assoc Lab Anim Sci *51*, 458-
1099 463.

1100 Li, G., and Cleland, T.A. (2017). A coupled-oscillator model of olfactory bulb gamma
1101 oscillations. PLoS Comput Biol *13*, e1005760.

1102 Linster, C., and Cleland, T.A. (2016). Neuromodulation of olfactory transformations.
1103 Curr Opin Neurobiol *40*, 170-177.

Lisman, J. (2005). The theta/gamma discrete phase code occuring during the hippocampal phase precession may be a more general brain coding scheme. Hippocampus *15*, 913-922.

Lisman, J., and Buzsaki, G. (2008). A neural coding scheme formed by the combined function of gamma and theta oscillations. Schizophr Bull *34*, 974-980.

Lisman, J.E., and Idiart, M.A. (1995). Storage of 7 +/- 2 short-term memories in oscillatory subcycles. Science *267*, 1512-1515.

Lisman, J.E., and Jensen, O. (2013). The theta-gamma neural code. Neuron *77*, 1002-1016.

Litwin-Kumar, A., Harris, K.D., Axel, R., Sompolinsky, H., and Abbott, L.F. (2017). Optimal Degrees of Synaptic Connectivity. Neuron *93*, 1153-1164 e1157.

Martin, C., Gervais, R., Chabaud, P., Messaoudi, B., and Ravel, N. (2004). Learning-induced modulation of oscillatory activities in the mammalian olfactory system: the role of the centrifugal fibres. J Physiol Paris *98*, 467-478.

Martin, C., Gervais, R., Messaoudi, B., and Ravel, N. (2006). Learning-induced oscillatory activities correlated to odour recognition: a network activity. Eur J Neurosci *23*, 1801-1810.

Martin, C., and Ravel, N. (2014). Beta and gamma oscillatory activities associated with olfactory memory tasks: different rhythms for different functional networks? Front Behav Neurosci *8*, 218.

Marton, C.D., Fukushima, M., Camalier, C.R., Schultz, S.R., and Averbeck, B.B. (2019). Signature Patterns for Top-Down and Bottom-Up Information Processing via Cross-Frequency Coupling in Macaque Auditory Cortex. eNeuro *6*.

Mizuseki, K., Sirota, A., Pastalkova, E., and Buzsaki, G. (2009). Theta oscillations provide temporal windows for local circuit computation in the entorhinal-hippocampal loop. Neuron *64*, 267-280.

Nguyen Chi, V., Muller, C., Wolfenstetter, T., Yanovsky, Y., Draguhn, A., Tort, A.B., and Brankack, J. (2016). Hippocampal Respiration-Driven Rhythm Distinct from Theta Oscillations in Awake Mice. J Neurosci *36*, 162-177.

Niv, Y., Daniel, R., Geana, A., Gershman, S.J., Leong, Y.C., Radulescu, A., and Wilson, R.C. (2015). Reinforcement learning in multidimensional environments relies on attention mechanisms. J Neurosci *35*, 8145-8157.

O'Keefe, J., and Recce, M.L. (1993). Phase relationship between hippocampal place units and the EEG theta rhythm. Hippocampus *3*, 317-330.

Osinski, B.L., and Kay, L.M. (2016). Granule cell excitability regulates gamma and beta oscillations in a model of the olfactory bulb dendrodendritic microcircuit. J Neurophysiol, jn 00988 02015.

Pakan, J.M., Francioni, V., and Rochefort, N.L. (2018). Action and learning shape the activity of neuronal circuits in the visual cortex. Curr Opin Neurobiol *52*, 88-97.

1143 Pouille, F., and Schoppa, N.E. (2018). Cannabinoid Receptors Modulate Excitation of
1144 an Olfactory Bulb Local Circuit by Cortical Feedback. Front Cell Neurosci *12*, 47.

1145 Ramirez-Gordillo, D., Ma, M., and Restrepo, D. (2018). Precision of Classification of
1146 Odorant Value by the Power of Olfactory Bulb Oscillations Is Altered by Optogenetic
1147 Silencing of Local Adrenergic Innervation. Front Cell Neurosci *12*, 48.

1148 Rebello, M.R., McTavish, T.S., Willhite, D.C., Short, S.M., Shepherd, G.M., and
1149 Verhagen, J.V. (2014). Perception of odors linked to precise timing in the olfactory
1150 system. PLoS Biol *12*, e1002021.

1151 Reinhart, R.M.G., and Nguyen, J.A. (2019). Working memory revived in older adults by
1152 synchronizing rhythmic brain circuits. Nat Neurosci *22*, 820-827.

1153 Rinberg, D., Koulakov, A., and Gelperin, A. (2006). Sparse odor coding in awake
1154 behaving mice. JNeurosci *26*, 8857-8865.

1155 Rojas-Libano, D., Frederick, D.E., Egana, J.I., and Kay, L.M. (2014). The olfactory bulb
1156 theta rhythm follows all frequencies of diaphragmatic respiration in the freely behaving
1157 rat. Front Behav Neurosci *8*, 214.

1158 Rojas-Libano, D., and Kay, L.M. (2008). Olfactory system gamma oscillations: the
1159 physiological dissection of a cognitive neural system. Cogn Neurodyn *2*, 179-194.

1160 Rokni, D., Hemmelder, V., Kapoor, V., and Murthy, V.N. (2014). An olfactory cocktail
1161 party: figure-ground segregation of odorants in rodents. Nat Neurosci *17*, 1225-1232.

1162 Rosero, M.A., and Aylwin, M.L. (2011). Sniffing shapes the dynamics of olfactory bulb
1163 gamma oscillations in awake behaving rats. Eur J Neurosci *34*, 787-799.

1164 Schoppa, N.E. (2006). Synchronization of olfactory bulb mitral cells by precisely timed
1165 inhibitory inputs. Neuron *49*, 271-283.

1166 Seymour, R.A., Rippon, G., and Kessler, K. (2017). The Detection of Phase Amplitude
1167 Coupling during Sensory Processing. Front Neurosci *11*, 487.

1168 Short, S.M., and Wachowiak, M. (2019). Temporal Dynamics of Inhalation-Linked
1169 Activity across Defined Subpopulations of Mouse Olfactory Bulb Neurons Imaged In
1170 Vivo. eNeuro *6*.

1171 Shusterman, R., Smear, M.C., Koulakov, A.A., and Rinberg, D. (2011). Precise olfactory
1172 responses tile the sniff cycle. Nat Neurosci *14*, 1039-1044.

1173 Siegle, J.H., and Wilson, M.A. (2014). Enhancement of encoding and retrieval functions
1174 through theta phase-specific manipulation of hippocampus. Elife *3*, e03061.

1175 Skaggs, W.E., McNaughton, B.L., Wilson, M.A., and Barnes, C.A. (1996). Theta phase
1176 precession in hippocampal neuronal populations and the compression of temporal
1177 sequences. Hippocampus *6*, 149-172.

1178 Slotnick, B.M., and Restrepo, D. (2005). Olfactometry with mice. In Current Protocols in
1179 Neuroscience, J.N. Crawley, C.R. Gerefen, M.A. Rogawski, D.R. Sibley, P. Skolnick,
1180 and S. Wray, eds. (New York: John Wiley and Sons, Inc), pp. 1-24

1181

Smear, M., Shusterman, R., O'Connor, R., Bozza, T., and Rinberg, D. (2011). Perception of sniff phase in mouse olfaction. Nature *479*, 397-400.

Soltesz, I., Bourassa, J., and Deschenes, M. (1993). The behavior of mossy cells of the rat dentate gyrus during theta oscillations in vivo. Neuroscience *57*, 555-564.

Stopfer, M., Bhagavan, S., Smith, B.H., and Laurent, G. (1997). Impaired odour discrimination on desynchronization of odour-encoding neural assemblies. Nature *390*, 70-74.

Stopfer, M., and Laurent, G. (1999). Short-term memory in olfactory network dynamics. Nature *402*, 664-668.

Tort, A.B., Komorowski, R., Eichenbaum, H., and Kopell, N. (2010). Measuring phase-amplitude coupling between neuronal oscillations of different frequencies. J Neurophysiol *104*, 1195-1210.

Tort, A.B.L., Ponsel, S., Jessberger, J., Yanovsky, Y., Brankack, J., and Draguhn, A. (2018). Parallel detection of theta and respiration-coupled oscillations throughout the mouse brain. Sci Rep *8*, 6432.

van Wingerden, M., van der Meij, R., Kalenscher, T., Maris, E., and Pennartz, C.M. (2014). Phase-amplitude coupling in rat orbitofrontal cortex discriminates between correct and incorrect decisions during associative learning. J Neurosci *34*, 493-505.

1200 Vizcay, M.A., Duarte-Mermoud, M.A., and Aylwin Mde, L. (2015). Odorant recognition
1201 using biological responses recorded in olfactory bulb of rats. Comput Biol Med *56*, 192-
1202 199.

1203 Zelano, C., Jiang, H., Zhou, G., Arora, N., Schuele, S., Rosenow, J., and Gottfried, J.A.
1204 (2016). Nasal Respiration Entrains Human Limbic Oscillations and Modulates Cognitive
1205 Function. J Neurosci *36*, 12448-12467.

1206 Zhuang, L., Zhang, B., Qin, Z., and Wang, P. (2019). Nasal Respiration is Necessary for
1207 the Generation of gamma Oscillation in the Olfactory Bulb. Neuroscience *398*, 218-230.

1208

1209

1210

1211

1212
1213

1214

1215

1216

1217

1218

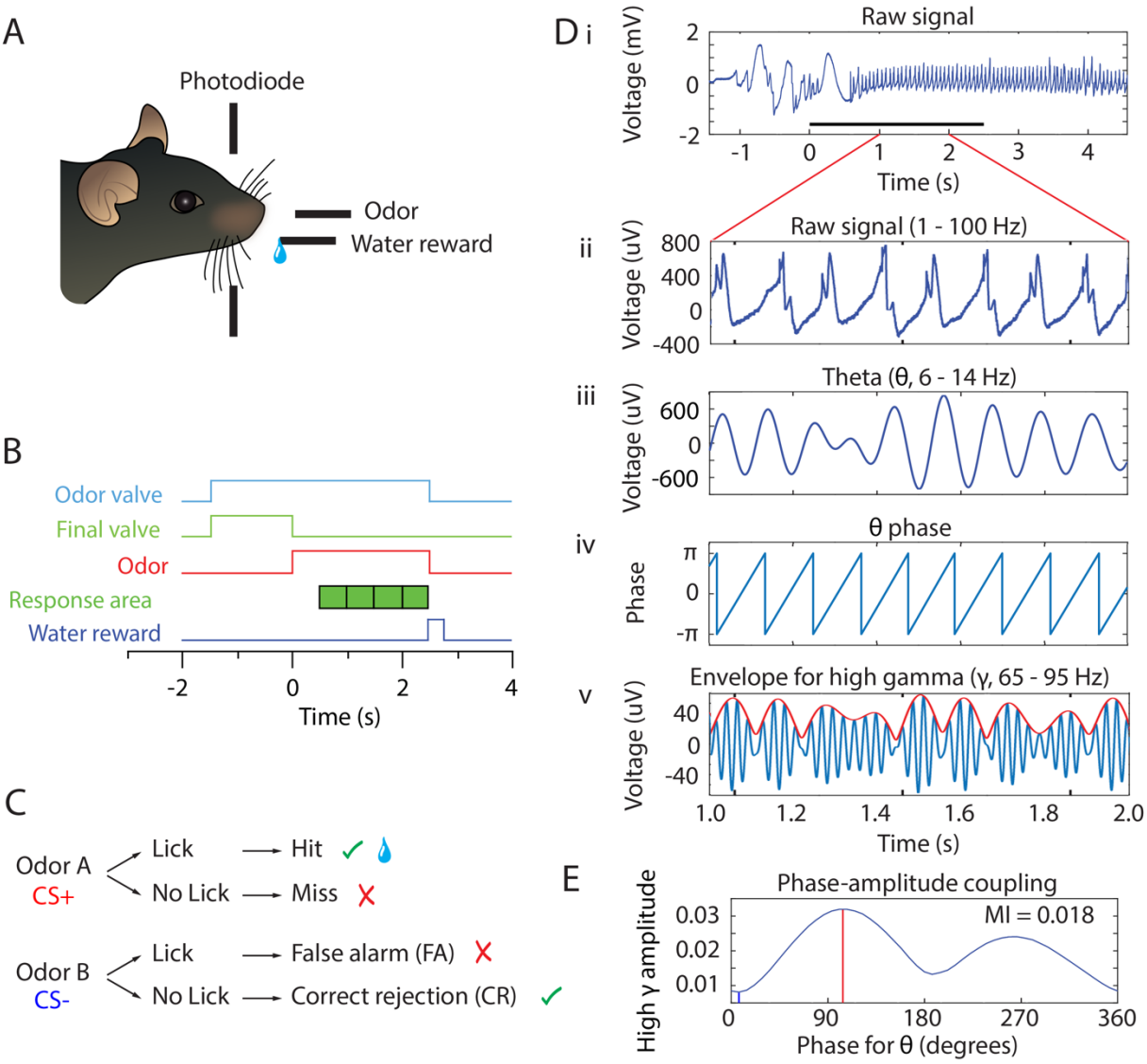

Figure 1. Behavioral task and PAC analysis.

(A) Behavioral apparatus. Mouse self-initiates trials by breaking a photodiode beam. Odorants and water are delivered according to the timeline in B and the decision tree in C.

(B) Timeline for a single trial. When the animal enters the port the air flow is diverted by turning the final valve output to the exhaust and the odorant valve is turned on. At this time the odor builds up to steady-state concentration flowing away from the animal for 1-1.5 seconds. At time 0 the final valve air flow is turned towards the odor port for 2.5 s

resulting in odor onset 100 ms after the valve is actuated. In order to trigger water reward for the rewarded odorant the mouse must lick at least once during each 0.5 s block for four blocks in the response area. If the stimulus is rewarded and the animal licked appropriately, a water reward is delivered.

(C) Decision tree for each stimulus. Green check mark means the correct decision was made. Red “X” mark indicates an incorrect decision. Water reward is represented by the water droplet symbol in the case of a hit.

(D) PAC data analysis of the LFP. For each electrode, raw signal collected at 20 kHz (i) is bandpass filtered to 1-100 Hz for broadband LFP (ii) or filtered into different frequency bands as needed (e.g. theta 6-14 Hz in iii or high gamma 65-95 Hz in v, blue line). Hilbert transform is used to calculate the theta phase (iv) and the amplitude envelope of higher oscillations such as high gamma (65-95 Hz) (red line in v). Theta phase and the envelope of the amplitude of high gamma are then used to calculate the probability for high gamma amplitude at specific phases of theta (PAC, shown in E).

(E) Probability for high gamma amplitude at specific phases of theta. In this example, PAC is strongest at ~100° and 270°. The coupling strength is quantified by the modulation index, MI. Peak phase (the phase of theta with the highest amplitude in high gamma) is indicated with a red line and trough phase is indicated with a blue line.

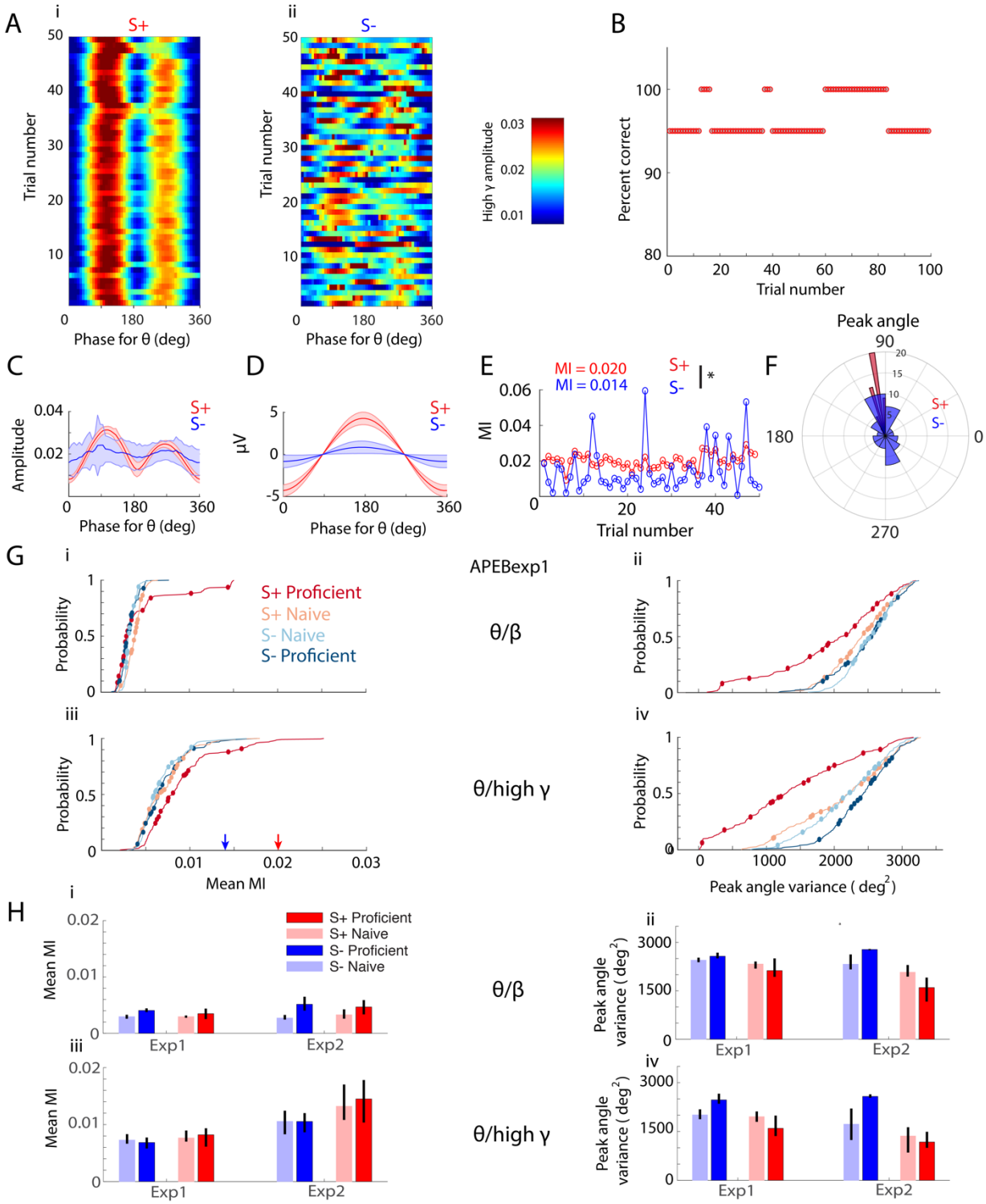

Figure 2. The peak angle variance of PAC changes as the animal learns to discriminate odorants.

1252 (A-F) Example of theta/high gamma phase amplitude coupling for a proficient animal
1253 (IAAPexp1 odorant pair).
1254 (A) Pseudocolor plots showing the phase amplitude relationship for S+ (left) and S-
1255 (right) for an example go no-go session. PAC between theta (6-14 Hz) phase and high
1256 gamma (65-95 Hz) amplitude was more variable for S- compared to S+.
1257 (B) Behavioral performance for this session. Over 100 trials, this trained animal
1258 discriminated between isoamyl acetate and acetophenone with 95-100% accuracy.
1259 (C) Theta phase distribution for high gamma amplitude (mean ± CI) for S+ (red) and S-
1260 (blue).
1261 (D) Mean theta LFP (mean ± CI) for one cycle for S+ (red) and S- (blue).
1262 (E) MI per trial for S+ (red) and S- (blue) as a function of trial number. The difference in
1263 MI between S+ and S- is statistically significant (ranksum p value < 0.001, n=50 S-
1264 trials, 49 S+ trials).
1265 (F) Polar histograms for high gamma peak theta angles for S+ (red) and S- (blue).
1266 (G) Cumulative histograms showing the differences in mean MI (i,iii) and peak angle
1267 variance (ii,iv) for theta/beta PAC (i,ii) and theta/high gamma PAC (iii,iv) for the APEB
1268 odorant in Exp1 for the S+ and S- odorants for naïve and proficient trial ranges. Peak
1269 angle variance for S+ displays a substantial decrease with learning, while mean MI
1270 shows small changes. Changes with learning and between events for mean MI and
1271 peak angle variance are statistically significant (GLM p value < 0.001, 896 d.f. for
1272 theta/beta and theta/high gamma, 16 electrodes per mouse, 14 mice). Blue and red
1273 arrows in Giii are MIs derived from the single-session example in C.

(H) Bar graph displaying mean MI (i,iii) and peak angle variance (ii,iv) for naïve and proficient trial ranges and S+ and S- events for mean values calculated per experiment for theta/beta (i,ii) and theta/high gamma PAC (iii,iv). GLM yielded significant p values for peak angle variance for theta/high gamma PAC for S+ vs. S- (< 0.01, 16 d.f.) and for the interaction between S+ vs. S- and proficiency ($p<0.05$, 16 d.f.). GLM yielded significant p values for peak angle variance for theta/beta PAC for S+ vs. S- and experiment and for the interaction between S+ vs. S- and experiment (< 0.01, 16 d.f.). For mean MI theta/high gamma PAC GLM yields significant difference for experiments ($p<0.01$, 16 d.f.). Finally, there are no significant effects for mean MI for theta/beta PAC ($p>0.05$, 16 d.f.) and no post hoc tests yield significant differences ($p>pFDR$).

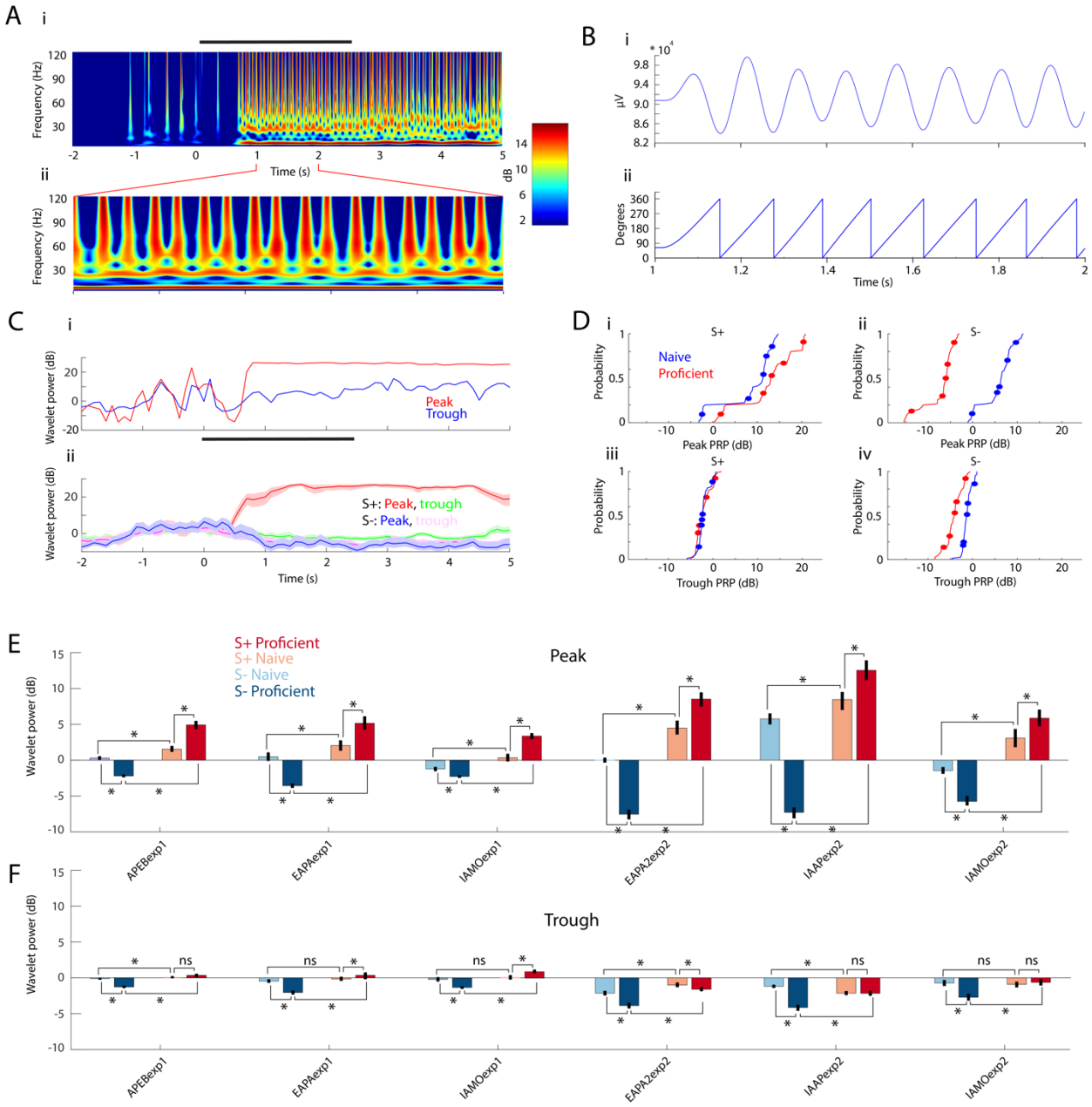

Figure 3. PRP increases for S+ and decreases for S- over learning.

(A) Example wavelet broadband LFP spectrogram for one S+ trial. Right: Pseudocolor scale for LFP power (in dB). Black bar represents the odor stimulation epoch (2.5 s). i: Full trial length demonstrating pre-odor baseline LFP, odor driven LFP, and reward epoch. ii: One-second epoch during odor stimulation.

1299 (B) i: Theta waveform (6-14 Hz) during odor stimulation. ii: Theta phase, extracted with
1300 Hilbert transform.
1301 (C) i: Single trial wavelet power referenced to either peak (108°, red) or trough (0°, blue)
1302 of the high gamma amplitude distribution along the theta phase. ii: PRP (± CI) averaged
1303 across the entire session for S+ and S-. Peak PRP for S+ displays the largest odor-
1304 induced increase in power that is sustained after the end of odor stimulation.
1305 (D) The thin lines are cumulative histograms for PRP for the LFP recorded in each
1306 electrode averaged for theta/high gamma for all proficient or naïve trials for mice
1307 performing to differentiate odorants in the IAAPexp2 odorant pair. i and ii are peak PRP
1308 and iii and iv are trough PRP. i and iii are S+; ii and iv are S-. As the animals learn the
1309 task, peak PRP (i and ii) increases for S+ and decreases for S-, whereas trough PRP (iii
1310 and iv) is relatively stable. The differences were statistically significant between peak
1311 and trough, S+ and S- and naïve and proficient (GLM p values < 0.001, 1016 d.f.).
1312 Circles are per mouse averages for PRP.
1313 (E-F) Odor-induced changes in high gamma PRP averages for all odorant pairs
1314 evaluated per electrode during the odor delivery epoch (0.5 – 2.5 s). Peak PRP (E)
1315 increases for S+ and decreases for S- when the mice become proficient. Trough PRP
1316 changes (F) are markedly weaker, yet they follow a similar trend (GLM p value < 0.001,
1317 6386 d.f. for S+ vs. S-, peak vs. trough, naïve vs. proficient). In addition, the learning-
1318 induced changes in PRP are larger in Exp2 (GLM p value < 0.001 for experiment, 6386
1319 d.f.).
1320
1321

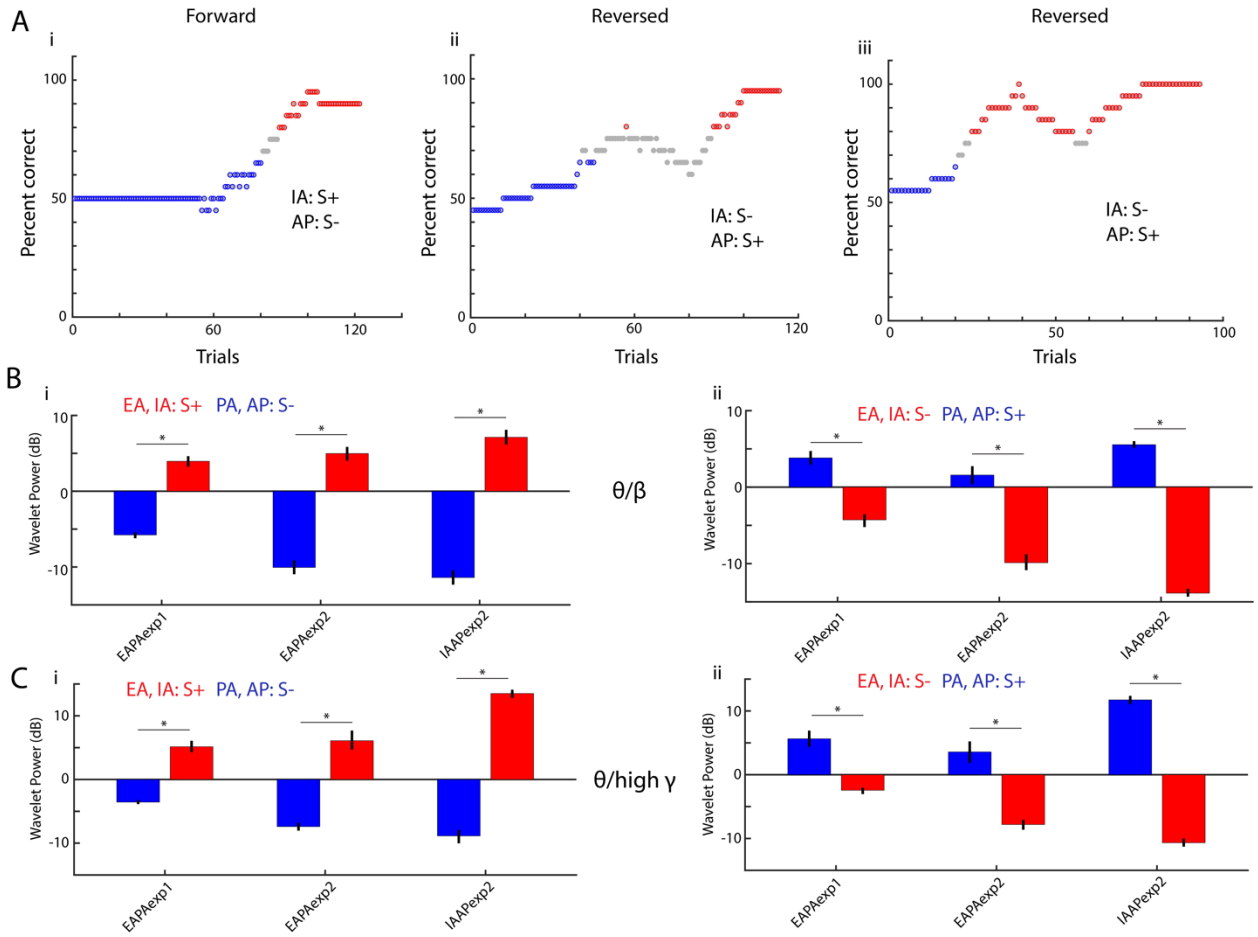

Figure 4. Peak theta-phase referenced power switches when odorant valence is reversed.

(A) Behavioral performance in three go-no go sessions for a mouse learning to differentiate the IAAPexp1 odorant pair. In the first session the rewarded odorant (S+) was isoamyl acetate (IA) and the unrewarded odorant (S-) was acetophenone (AP). In the other two sessions the valence of the odorant was reversed.

(B-C) Theta/beta (B) and theta/high gamma (C) peak PRP, calculated for trails when the mouse is proficient, switches when odorant valence is reversed. The data are shown for three odor pairs: EAPAexp1 (11 mice), EAPAexp2 (9 mice), IAAPexp2 (3 mice). GLM analysis yields significant changes for odorant, reversal and the interaction of reversal

1333 and odorant ($p<0.001$, 1051 d.f.). Asterisks denote post hoc significant differences

1334 ($p<pFDR=0.04$).

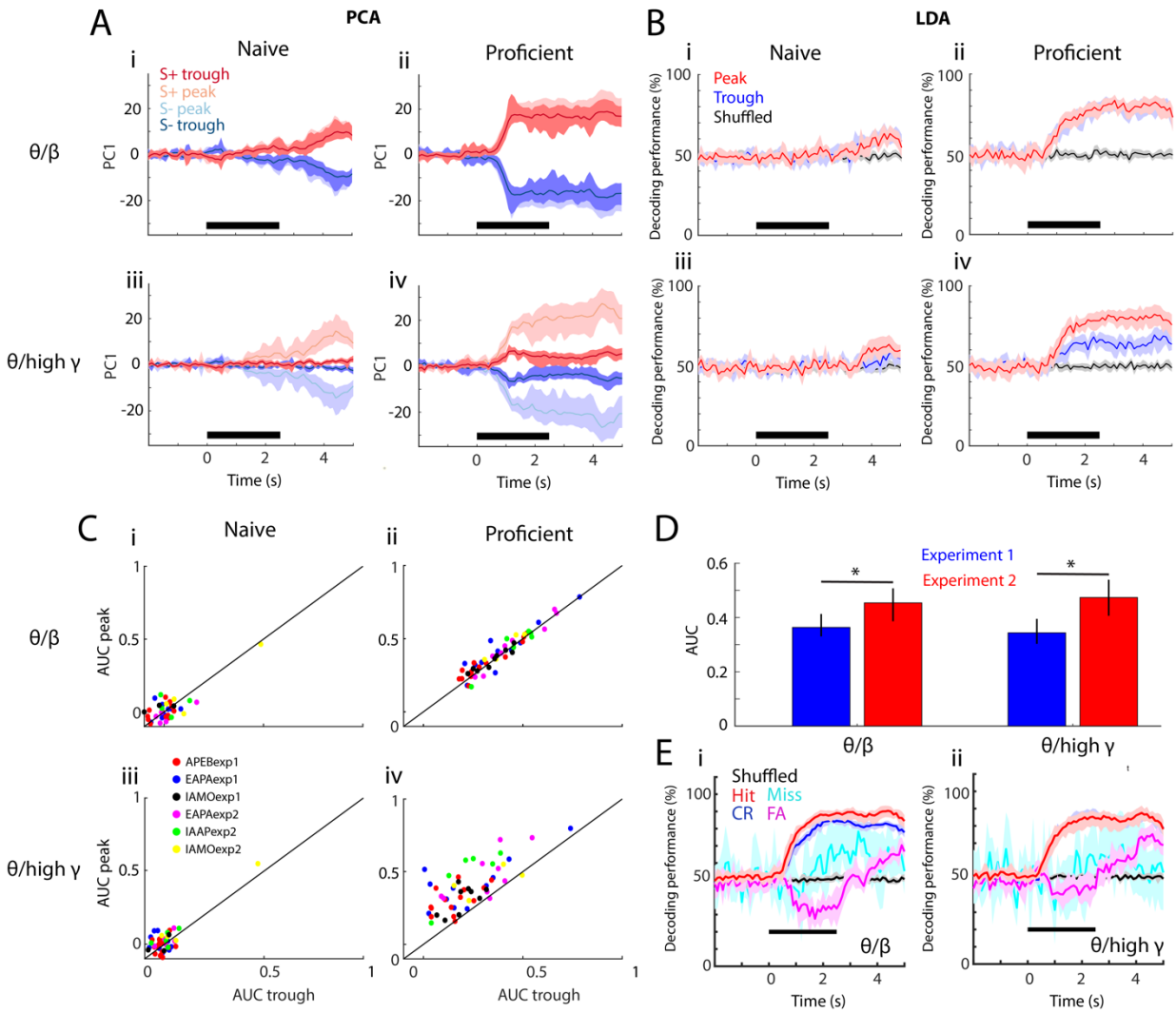

Figure 5. Linear discriminant analysis classifies stimuli using peak PRP.

(A-B) PCA (in panel A) and linear discriminant analysis (LDA; in panel B) of averaged PRP data for one example odorant pair, APEBexp1.

(A) PCA of PRP data from naïve (i,iii) to proficient (ii,iv)—i,ii: theta/beta, iii,iv: theta/high gamma. Both PRPs for S+ and S- are discriminable with learning.

(B) Decoding performance for the LDA of PRP data over learning (i,iii: naïve, ii,iv: proficient). i,ii: theta/beta, iii,iv: theta/high gamma. In the proficient state, LDA can decode stimulus identity using both PRPs (theta/beta PRP GLM naïve-proficient p value < 0.001, 104 d.f.; theta/high gamma PRP GLM naïve-proficient p value < 0.001, 104

d.f.). Peak and trough carry similar information for theta/beta; both peak- and trough-referenced beta power can be used to decode stimulus identity with learning. In theta/high gamma, peak PRP is significantly better at decoding the stimulus identity than trough PRP (GLM p value < 0.001, 104 d.f.), which is still better than shuffled data.

(C) Area under the curve (AUC) for peak versus trough PRP over task learning (i,iii: naïve, ii,iv: proficient) for all odorant pairs and experiments. i,ii: Theta/beta PRP. iii,iv: For theta/high gamma PRP GLM statistics show that peak AUC is significantly higher than trough (p value < 0.001 for 6 odorant pairs, 184 d.f.) and that there are significant changes over learning (p value < 0.001 for 6 odorant pairs, 184 d.f.). These data suggest that peak PRP decodes stimulus identity better than trough PRP.

(D) Average peak AUC (±CI) for all odorant pairs for theta/beta and theta/high gamma PRP for proficient mice for the two experimental settings. The learning-induced changes in PRP are larger in Exp2 (GLM p value < 0.05 for experiment, 102 d.f., *post hoc p<pFDR=0.03).

(E) Decoding performance for the LDA of PRP data for proficient mice calculated for the different behavioral outcomes of the go-no go task (Hit: red, Miss: cyan, CR: blue, FA: magenta, shuffled: black). i: Theta/beta PRP, ii: Theta/high gamma PRP. A GLM analysis indicates that there are significant differences between all behavioral outcomes except for Hit vs. CR for theta/high gamma (p<0.001 for all outcome pairs, except for Hit vs CR for theta/beta PRP that has p<0.01 and Hit vs. CR for theta/high gamma that has p>0.05, 2110 d.f.). There is no significant difference between experiments (GLM p>0.05, 2110 d.f.).

The lines in A,B and E are bounded by the bootstrapped 95% CI.

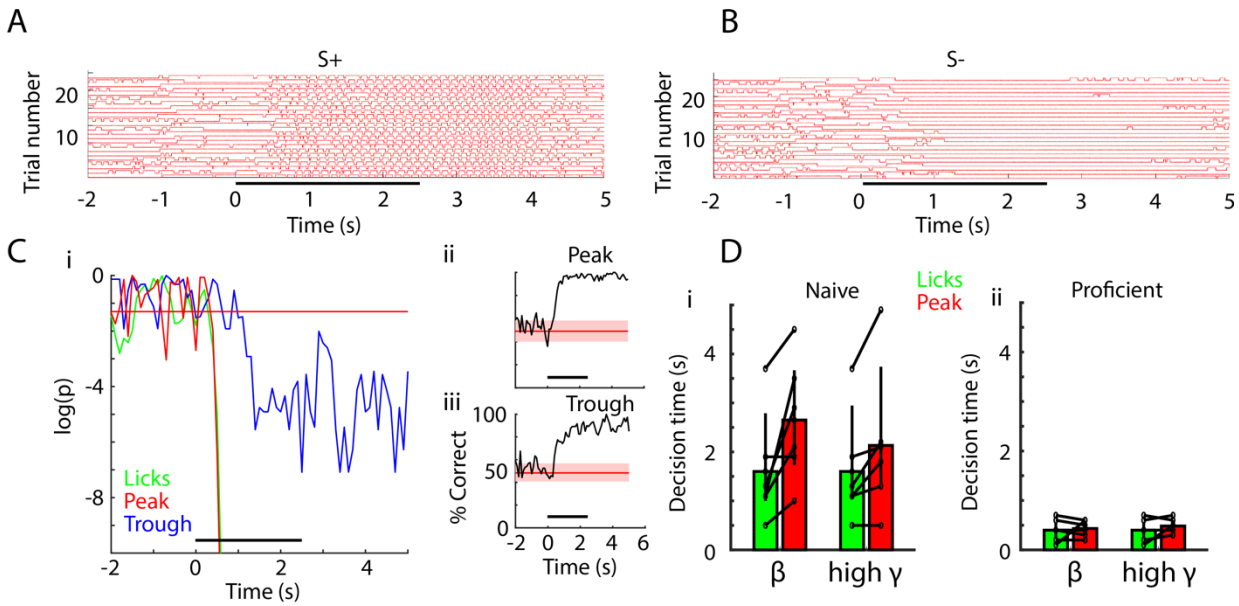

Figure 6. Decision-making time does not differ between licks and peak PRP LDA decoding of odorant identity

(A) Lick time course for 25 S+ trials in one session of EAPAexp2 for one proficient mouse. Horizontal black bar indicates odor delivery epoch for all time course subpanels**.**

(B) Lick time course for 25 S- trials in the same session as in A. Mouse refrains from licking in the presence of the unrewarded odorant.

(C) i: p value time courses for difference between S+ and S- for licks and peak PRP LDA predictions. ii and iii: decoding performance for PRP LDA. Decision making times for both licks and PRP LDA were calculated using data pooled for all mice performing odorant discrimination with the EAPAexp2 odorant pair. i: p value for the ranksum test compares the time-course for decision-making using licks for S+ vs. S- (green) or LDA prediction of odorant identity with peak (red) or trough (blue) PRP. This example illustrates that that peak PRP LDA prediction and lick divergence perform similarly, while LDA prediction with trough PRP is significantly slower in stimulus decoding.

Horizontal red line indicates p = 0.05. ii and iii: LDA decoding performance appears to be faster and more accurate using peak PRP (ii) vs. trough PRP (iii).

(D) Decision times for licks and for pooled animal peak theta/beta and theta/high gamma PRP LDA in naïve (i) and proficient (ii) mice. Decision times were significantly reduced with task learning (GLM p value < 0.001, 44 d.f.). Decision times for lick vs. PRP LDA and theta/beta vs. theta/high gamma did not differ (GLM p values > 0.05, 44 d.f.).

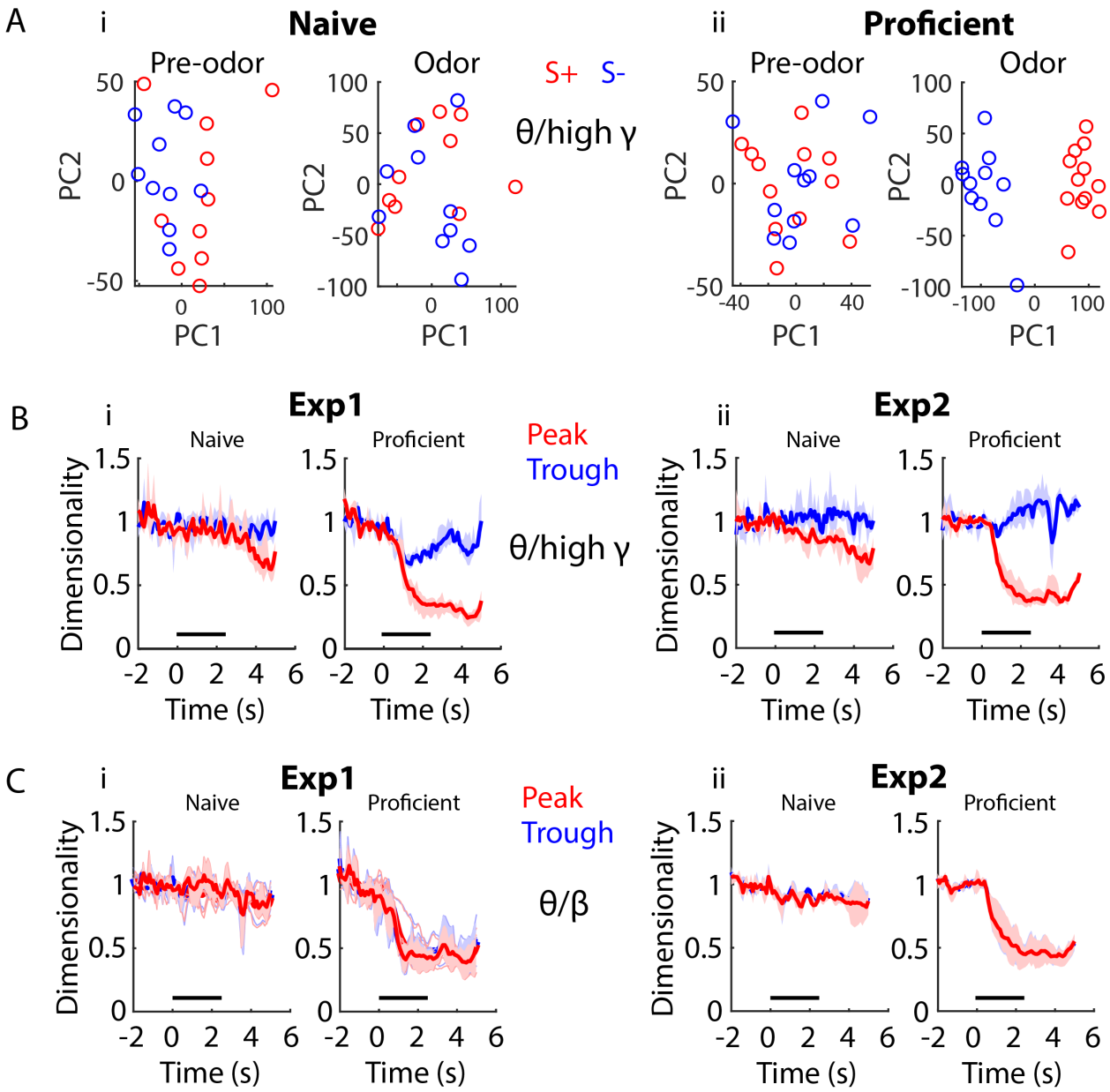

Figure 7. Dimensionality changes with learning and during the time course of the trial.

(A) Scatter plot showing the first two principal components for twenty trials of a PCA for peak theta/high gamma PRP recorded in mice learning to differentiate the odorants in the EAPAexp1 odorant pair. The input to the PCA was the peak PRP recorded in 16 electrodes pooled for all mice. Principal components are intermingled between S+ (red)

and S- (blue) trials in the naïve state (left) in pre-odor and odor-delivery epochs, yet they separate during odor delivery upon task acquisition (right). i. Naïve animals. ii. Proficient animals.

(B) Within-trial peak (red) and trough (blue) theta/high gamma PRP dimensionality time course for data pooled across mice is shown for Exp1 (i) and Exp2 (ii), normalized to pre-trial dimensionality. A GLM analysis indicates that there are significant differences for time course, proficient vs. naïve, experiments and peak vs. trough, and for pair interactions of these factors (GLM p values < 0.001, 1688 d.f.).

(C) Within-trial peak (red) and trough (blue) theta/beta PRP dimensionality time course for data pooled across mice is shown for Exp1 (i) and Exp2 (ii), normalized to pre-trial dimensionality. GLM analysis found statistically significant differences for time course, and proficient vs. naïve, and for interaction of these factors (GLM p values < 0.001, 1688 d.f.), and there was a statistically significant difference between experiments (GLM p value < 0.01, 1688 d.f.). However, there was no difference between peak and trough (GLM p value >0.05, 1688 d.f).

1416 **SUPPLEMENTAL INFORMATION**

1417 **Detailed evaluation of phase amplitude coupling on a per odorant pair basis.**

1418 Figure 2-figure supplement 2 A and B show the summary of changes with
1419 learning for S+ and S- odorants for MI (Ai, Bi) and the peak angle variance (Aii,Bii) for
1420 theta/beta (A) and theta/high gamma (B) for per electrode PAC for all odorant pairs.
1421 When evaluated on a per odorant pair basis theta/beta and theta/high gamma PAC
1422 strength, quantified as the MI calculated for LFPs recorded in each electrode, was
1423 stronger for recordings in Exp2 compared to Exp1, and there was a statistically
1424 significant increase in the MI for S+ with learning (naïve vs. proficient) (GLM analysis p
1425 value < 0.001, for event, proficiency and experiment, with the exception that p < 0.01 for
1426 proficiency for theta/high gamma, 3255 d.f., number of mice is in Table S1).
1427 Interestingly, there were decreases in peak angle variance for S+, and/or increases in
1428 peak angle variance for S- for theta/high gamma PAC when the animals became
1429 proficient (GLM analysis p values < 0.001 for event type, proficiency and experiment for
1430 both theta/beta and theta/high gamma, 3255 d.f., number of mice is in Table S1).

1431

1432 **Comparison of decision-making times calculated using pooled animal PRP LDA**
1433 **data vs. per animal data.**

1434 Figure 6-figure supplement 1 B and C show that for both lick (B) and PRP peak
1435 LDA (C) the decision-making time is faster when data are pooled for all mice. Lick
1436 decision-making times were significantly faster with pooled data (GLM p value < 0.01,
1437 21 d.f.) as were decision making times for peak PRP LDA (GLM p value < 0.01, 21 d.f.).

Because pooled animal data yield faster decision times we did the comparison of decision times in Figure 6 using pooled animal data.

1442 **Table S1. Odorant pairs, implant device, mouse genotype and electrode locations**

1443 **for each experiment**

Experiment	Implant	Coordinates	Genotype	Odorant pair	Odorant name	Odorant dilution (v/v)	Number of mice
Exp1	Optetrodes	+4.25 mm AP, +0.4 mm ML, -0.53 mm DV	DBH-Cre eNpHR3.0 (see Methods)	APEBexp1	Acetophenone	1%	14
					Ethyl benzoate	1%	
				EAPAexp1	Ethyl acetate (EA)	0.1%	11
					EA/Propyl acetate (PA)	0.05% EA + 0.05% PA	
				IAMOexp1	Isoamyl acetate	1%	9
					Mineral oil	100%	
Exp2	Tetrodes	+4.28 mm AP, +0.05 mm ML, -1.0 mm DV	C57BL/6	EAPAexp2	Ethyl acetate	1%	9
					Propyl acetate	1%	
				IAAPexp2	Isoamyl acetate	1%	6
					Acetophenone	1%	
				IAMOexp2	Isoamyl acetate	1%	4
					Mineral oil	100%	

1444

1445 Odorant identities for each pair are listed along with concentrations represented as

1446 volume/volume dilutions in mineral oil (MO). In the case of EAPAexp1, EA is 0.1% ethyl

1447 acetate and PA is a mixture of 0.05% ethyl acetate + 0.05% propyl acetate. The two

1448 recording locations (Exp1 and Exp2) are listed in millimeters with respect to bregma.

1449 Note: Cre expression can affect physiological parameters and therefore, the differences

1450 found between experiments in this publication can be due to Cre expression (Harno et

1451 al., 2013). However, it is not evident to us which of the methodological differences

1452 between experiments contributes to statistical differences in measured parameters.

1453

1454

		Odorant pair				
Experiment	Mouse ID	APEB	EAPA	IAAP	IAMO	
1	261365	2	2	N/A	2	
1	261366	2	2	N/A	2	
1	261367	2	2	N/A	2	
1	261368	2	2	N/A	2	
1	262641	2	2	N/A	2	
1	293851	0	2	N/A	0	
1	294213	0	2	N/A	0	
1	254071	2	2	N/A	2	
1	261032	2	2	N/A	2	
1	294211	0	2	N/A	0	
1	294212	0	2	N/A	0	
1	159868	2	0	N/A	0	
1	159863	2	0	N/A	0	
1	159865	2	0	N/A	0	
1	159866	2	0	N/A	0	
1	159867	2	0	N/A	0	
1	159869	2	0	N/A	0	
1	254072	2	0	N/A	2	
1	261036	0	0	N/A	2	Experiment 1 total
	Total per odorant pair	28	22	N/A	18	68
2	M4	N/A	0	5	0	
2	M5	N/A	0	2	0	
2	T0	N/A	1	3	0	
2	T2	N/A	1	4	0	
2	R2	N/A	2	0	2	
2	R3	N/A	3	0	0	
2	R4	N/A	3	0	3	
2	R5	N/A	4	0	4	
2	R6	N/A	2	0	2	
2	R8	N/A	1	3	0	
2	R9	N/A	2	4	0	Experiment 2 total
	Total per odorant pair	N/A	19	21	11	51
						Grand total
						119

Table S2. Total sessions per mouse, experiment, and odorant pair.
Odorant pair abbreviations derived from Table S1. The number of sessions are in the “odorant pair” columns. Each row represents one animal.

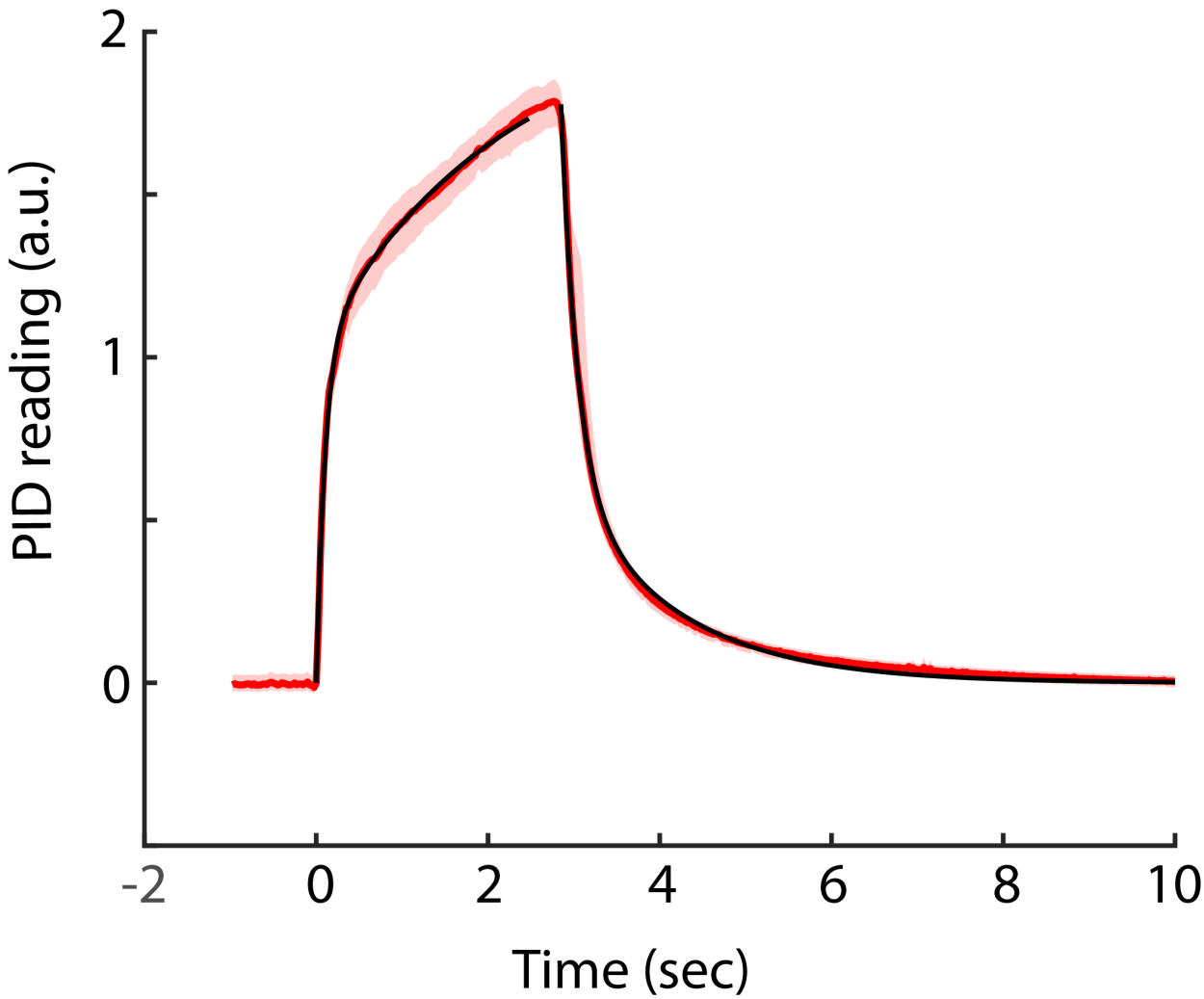

Figure 1-figure supplement 1. Time course for odorant concentration measured at the odor spout in the olfactometer. A miniPID (Aurora Scientific) photoionization detector was used to measure the concentration of odorant at the odor spout of the olfactometer. The odorant was air equilibrated with Sharpie black ink. The red line is the concentration of the odorant in arbitrary units bounded by the bootstrapped confidence interval (n=10 traces). Time was aligned to the onset of the increase in odorant concentration that took place 104.5±7 msec (mean±SD, n=10) after the final valve was diverted to deliver the odorant to the odorant spout. The black lines are regression fits of exponential increase and decrease lines with time constants of 0.12 and 2.16 sec

1465 (increase, two exponential terms) and 0.19 and 1.28 sec (decrease, two exponential

1466 terms).

1467

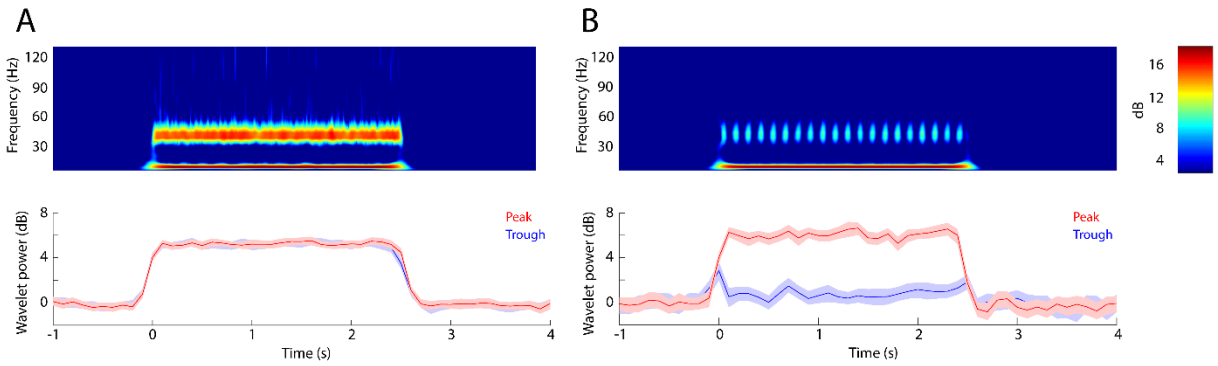

Figure 1-figure supplement 2. Simulation: PRP wavelet analysis for theta-gamma waves with/without PAC.

LFP data were generated by sinusoids supplemented with gaussian random noise. The data was analyzed for PRP as described in the text.

(A) Example with no theta/gamma PAC generated by input of two continuous cosine waves of 8 Hz and 40 Hz. Top: Morlet wavelet spectrogram shows a continuous increase in power at the two frequencies. Bottom: peak (red) and trough (blue) PRP do not differ. MI = 0.0004.

(B) Example of theta/gamma PAC generated with input of 40 Hz gamma bursts placed at the 180° phase of an 8 Hz theta sine wave (the bursts take place at the peak of PAC). Top: Morlet wavelet spectrogram shows discrete increases of gamma power and a continuous increase in power at 8 Hz. Bottom: peak (red) PRP shows a large increase in power while trough PRP (blue) does not increase. MI = 0.01.

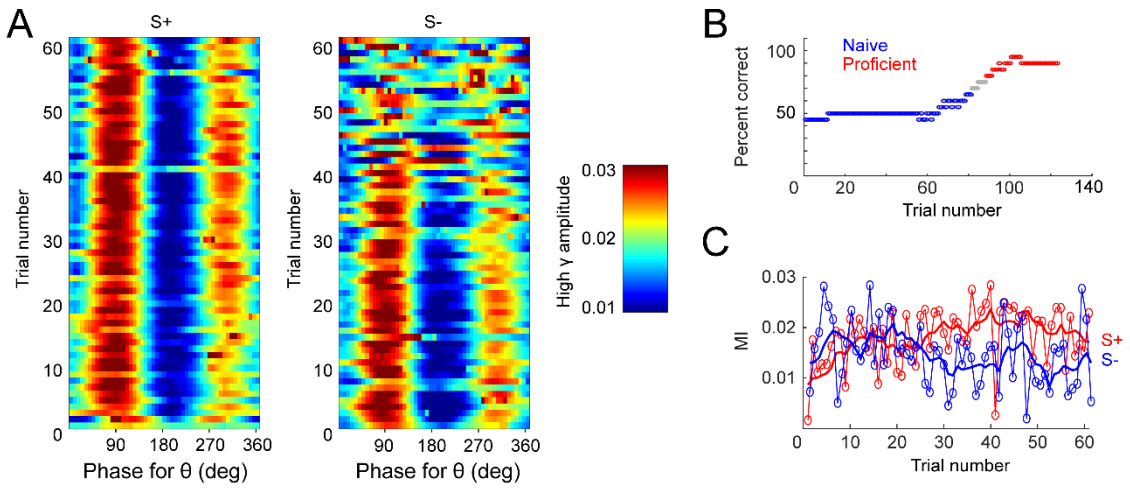

Figure 2-figure supplement 1. Example of PAC changes over learning in one session.

(A) PAC for all S+ trials (left) and S- trials (middle), with high γ amplitude color bar quantified at right.

(B) Behavioral performance. Mouse starts the session performing at chance, then learns the task, acquiring proficiency by the end. Blue: naïve, performance ≤ 65%. Red: proficient, performance ≥ 80%.

(C) PAC quantified as mean MI for S+ (red) and S- (blue). With learning, PAC increases for S+ and decreases for S-.

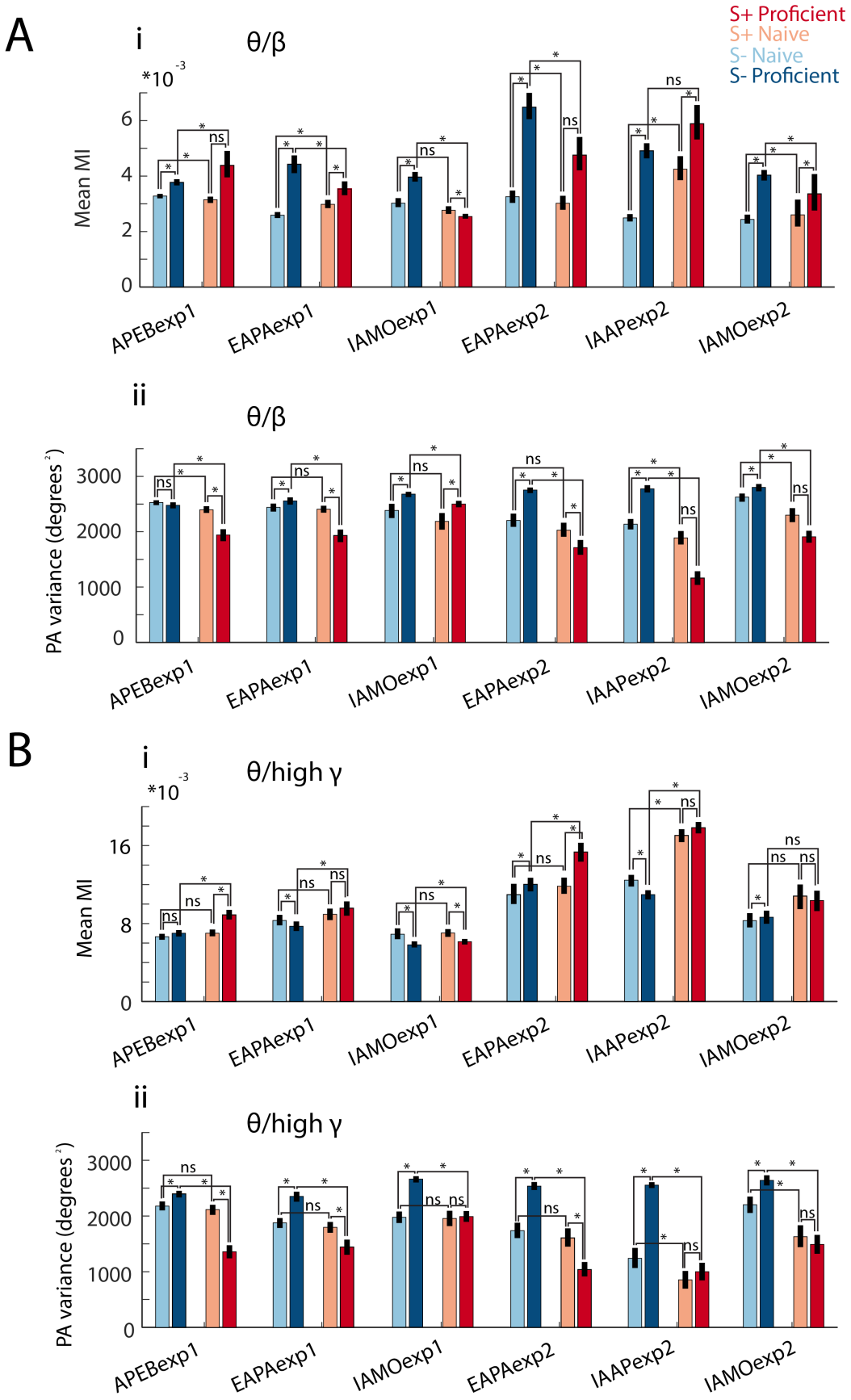
A
i
θ/β
*10^-3
Mean MI
S+ Proficient
S+ Naive
S- Naive
S- Proficient
APEBexp1
EAPAexp1
IAMOexp1
EAPAexp2
IAAPexp2
IAMOexp2
ii
θ/β
PA variance (degrees²)
B
i
θ/high γ
*10^-3
Mean MI
ii
θ/high γ
PA variance (degrees²)

1498

1499 **Figure 2-figure supplement 2. Modulation index and peak angle variance shown**
1500 **for each odorant pair.**
1501 Bar graphs displaying for theta/beta (A) and theta/high gamma (B) PAC differences in
1502 mean MI (Ai and Bi) and peak angle variance (Aii and Bii) between naïve and proficient
1503 trial ranges and S+ and S- events for all sessions for all the odorant pairs. GLM yielded
1504 significant p values (< 0.001) for both mean MI and peak angle variance for event,
1505 proficiency and experiment, with the exception that p < 0.01 for proficiency for theta/high
1506 gamma (3255 d.f., number of mice is in Table S1). Asterisks denote a significant post-
1507 hoc difference evaluated with either a t-test or a ranksum test (p < pFDR, for the
1508 number of mice per odorant, see Table S1). Changes in mean MI were variable for
1509 different odorants. MI displays differences between events and learning states that differ
1510 in magnitude between odorant pairs. Peak angle variance (at right) increases with task
1511 proficiency for S- and decreases for S+ for all odorants.
1512
1513

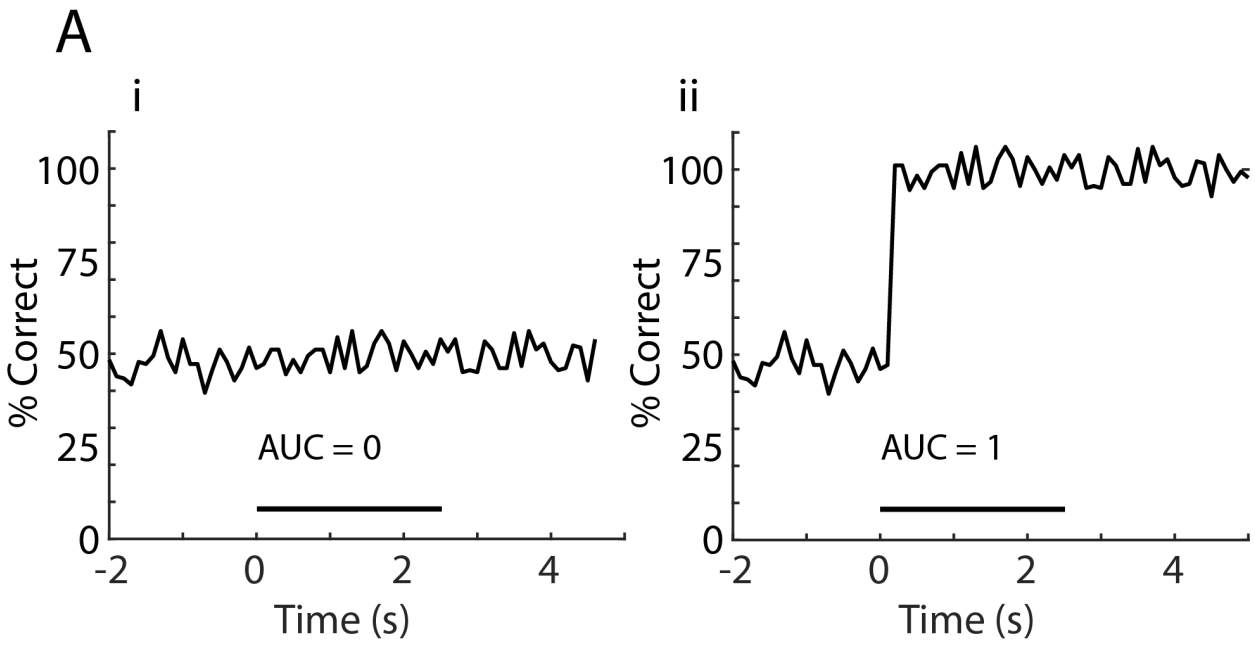

Figure 5-figure supplement 1. Simulated LDA performance data illustrating AUC zero and one.

(A) Simulated data illustrating the time course for decoding performance for LDA for discrimination of odor identity with: i, The area under the curve (AUC) = 0, LDA was not able to identify the stimuli, and ii, AUC = 1, perfect identification of the stimulus after odor application. AUC was calculated as the area under the curve during odorant stimulation normalized to 1.

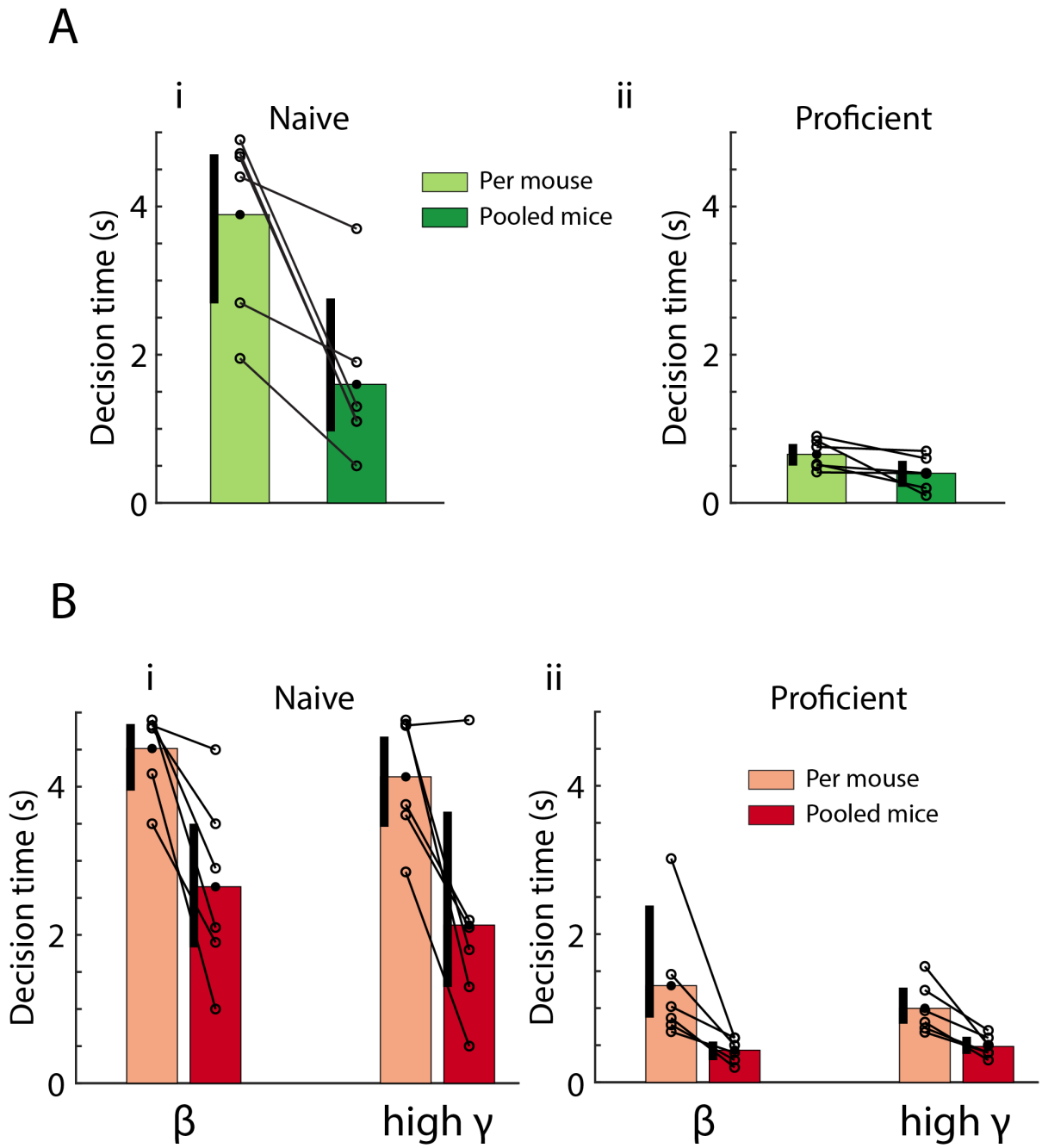

Figure 6-figure supplement 1. Decision times are faster for peak PRP LFP LDA computed when data are pooled across mice.

(A) Comparison of lick decision times between per mouse (light green) vs. pooled mouse (dark green) p value estimates. GLM p value for the difference in lick decision times between per-mouse vs. pooled GLM < 0.01, 20 d.f.

1530 (B) Decision times for peak PRP decoding of stimulus identity for the per mouse (light
1531 red) vs. pooled mouse (red) LDA for naïve (i) vs. proficient (ii) mice. For both theta/beta
1532 and theta/high gamma decoding of stimulus identity via peak PRP is faster using data
1533 pooled across mice than the per mouse estimate (GLM p values < 0.001, 20 d.f.). There
1534 is no difference in decision-making times between theta/beta and theta/high gamma
1535 (GLM p values > 0.05, 20 d.f.).
1536 Vertical black bars represent the 95% bootstrap confidence interval of the data in each
1537 condition; they are shifted to the left to better display the mean and individual odorant
1538 pair values.

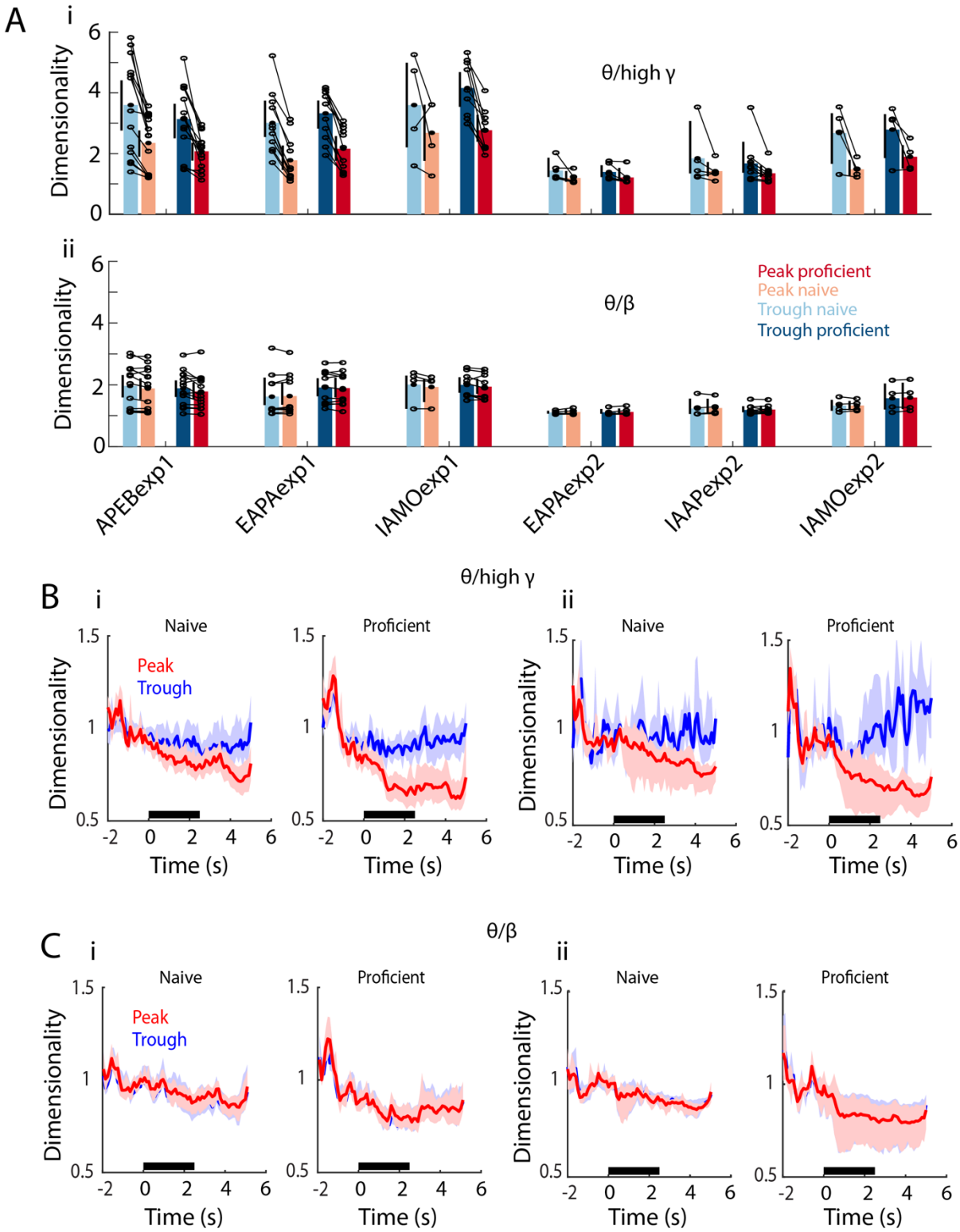

1539

1540 **Figure 7-figure supplement 1. PRP dimensionality estimated per mouse.**

(A) Per mouse theta/high gamma (i) and theta/beta (ii) PRP dimensionality summary for all six odorant pairs calculated before odorant delivery. GLM p value < 0.001 for Exp1 vs. Exp2 and > 0.05 for peak vs. trough, 379 d.f.

(B) Per mouse examples of the time course of theta/high gamma PRP dimensionality for APEBexp1 (i) and IAMOexp2 (ii). A GLM analysis of the dimensionality for peak PRP LFP calculated on a per mouse basis for all odorant pairs indicates that there are significant differences in theta/high gamma peak PRP LFP dimensionality for proficient vs. naïve, time, Exp1 vs. Exp2 and for interactions of these factors (except for the interaction of Exp1 vs. Exp2 x proficient vs. naïve) (GLM p values < 0.001, 6098 d.f.).

(C) Per mouse examples of the time course of theta/beta PRP dimensionality for APEBexp1 (i) and IAMOexp2 (ii). A GLM analysis of the dimensionality for theta/beta peak PRP LFP calculated on a per mouse basis for all odorant pairs indicates that there are significant differences for proficient vs. naïve, time, Exp1 vs. Exp2 and for interactions of these factors (GLM p values < 0.01, 6098 d.f.).

For theta/high gamma peak PRP LFP dimensionality there was a statistically significant difference between peak and trough (GLM p value < 0.0001, 12196 d.f.). and for theta/beta peak PRP LFP dimensionality there was no difference between peak and trough (GLM p value > 0.05, 12196 d.f.).